

Machine-learning-based estimates of global natural vegetated wetland methane emissions (2000-2025)

Mengze Li^{1,2}, Robert B. Jackson^{3,3}, Marielle Saunois⁴, Philippe Ciais⁴, Ben Poulter⁵, Josep G. Canadell⁶, Prabir K. Patra^{7,8}, Hanqin Tian^{9,10}, Zhen Zhang¹¹, Etienne Fluet-Chouinard¹², Zutao Ouyang¹³, Ting Zhang¹, David J. Beerling¹⁴, Dmitry A. Belikov¹⁵, Philippe Bousquet⁴, Danilo Custodio⁴, Naveen Chandra⁷, Xinyu Dou², Nicola Gedney¹⁶, Peter O. Hopcroft¹⁷, Alison M. Hoyt², Kazuhito Ichii^{15,18}, Akihito Ito¹⁹, Atul K. Jain²⁰, Katherine Jensen²¹, Fortunat Joos²², Thomas Kleinen²³, Masayuki Kondo^{8,24}, Fa Li², Tingting Li²⁵, Xiangyu Liu²⁶, Shamil Maksyutov²⁷, Avni Malhotra²⁸, Adrien Martinez⁴, Kyle McDonald²¹, Joe R. Melton²⁹, Jurek Müller²², Yosuke Niwa^{27,30}, Shufen Pan⁹, Shushi Peng³¹, Changhui Peng^{32,33}, Zhangcai Qin³⁴, Peter Raymond³⁵, William Riley³⁶, Arjo Segers³⁷, Rona L. Thompson¹⁶, Aki Tsuruta³⁸, Xi Yi⁴, Kunxiaojuan Yuan³⁹, Wenxin Zhang³⁰, Bo Zheng^{40,41}, Qing Zhu³⁶, Qian Zhu⁴², Qianlai Zhuang²⁶

- 1 Department of Geography, National University of Singapore, Singapore.
- 2 Stanford Doerr School of Sustainability, Department of Earth System Science, Stanford, CA, USA.
- 3 Department of Earth System Science, Woods Institute for the Environment, and Precourt Institute for Energy, Stanford University, Stanford, CA, USA.
- 4 Laboratoire des Sciences du Climat et de l'Environnement (LSCE), CEA, CNRS, UVSQ, Université Paris Saclay, Gif-sur-Yvette, France.
- 5 Spark Climate Solutions, San Francisco, CA, USA.
- 6 Global Carbon Project, CSIRO Environment, ACT 2601, Australia.
- 7 Research Institute for Global Change, JAMSTEC, 3173-25 Showa-machi, Kanazawa, Yokohama, 236-0001, Japan.
- 8 Seto Inland Sea Carbon Neutral Research Center (S-CNC), Hiroshima University, Higashi-Hiroshima, Hiroshima 739-8529, Japan.
- 9 Center for Earth System Science and Global Sustainability, Schiller Institute for Integrated Science and Society, Boston College, Chestnut Hill, MA, USA.
- 10 Department of Earth and Environmental Sciences, Boston College, Chestnut Hill, USA.
- 11 State Key Laboratory of Tibetan Plateau Earth System, Environment and Resources, and Institute of Tibetan Plateau Research, Chinese Academy of Sciences, Beijing, China.
- 12 Earth System Science Division, Pacific Northwest National Laboratory, Richland, WA, USA.
- 13 College of Forestry, Wildlife and Environment, Auburn University, Auburn, AL, USA.
- 14 School of Biosciences, University of Sheffield, U.K.
- 15 Center for Environmental Remote Sensing, Chiba University, Chiba, Japan.
- 16 MetOffice Hadley Centre, Joint Centre for Hydrometeorological Research, Wallingford, U.K.
- 17 School of Geography, Earth & Environmental Sciences, University of Birmingham, U.K.
- 18 Graduate School of Science and Engineering, Chiba University, 1-33, Yayoi-cho, Inage-ku, Japan.
- 19 Graduate School of Agricultural and Life Sciences, The University of Tokyo, Tokyo, Japan.
- 20 Department of Climate, Meteorology, and Atmospheric Sciences, University of Illinois at Urbana-Champaign, Urbana, IL, USA.
- 21 Department of Earth and Atmospheric Sciences, City University of New York, New York, NY, USA.
- 22 Climate and Environmental Physics, Physics Institute and Oeschger Centre for Climate Change Research, University of Bern, Bern, Switzerland.
- 23 Max Planck Institute for Meteorology, Hamburg, Germany.

Style Definition: Normal

Style Definition: Heading 1

Style Definition: Heading 2

Style Definition: Heading 3

Style Definition: Heading 4

Style Definition: Bullets

Deleted: Global natural

Formatted: Normal, Space Before: 9 pt, Border: Top: (No border), Bottom: (No border), Left: (No border), Right: (No border), Between : (No border)

Formatted: Font colour: Black

Deleted: Paul Miller⁹⁰,

Deleted: ^{27,31},

Deleted: Peng³²,

Deleted: Peng^{33,34},

Deleted: Qin³⁵,

Deleted: Raymond³⁶,

Deleted: Riley³⁷,

Deleted: Segers³⁸,

Deleted: Tsuruta³⁹,

Deleted: Yuan⁴⁰,

Deleted: Zheng^{41,42},

Deleted: Zhu³⁷,

Deleted: Zhu⁴³,

Formatted: Font colour: Black

Formatted: Normal, Space Before: 6 pt, Border: Top: (No border), Bottom: (No border), Left: (No border), Right: (No border), Between : (No border)

Deleted: 1

Formatted: Font colour: Black

Formatted: Normal, Border: Top: (No border), Bottom: (No border), Left: (No border), Right: (No border), Between : (No border), Tab stops: 7.96 cm, Centred + 15.92 cm, Right

- 59 24 The IDEC Institute - Center for Peaceful and Sustainable Futures (CEPEAS), Network for Education and Research on
60 Peace and Sustainability (NERPS), Graduate School of Humanities and Social Sciences International Economic
61 Development Program (IEDP), Graduate School of Innovation and Practice for Smart Society (SmaSo), Hiroshima
62 University, Higashi-Hiroshima, Hiroshima 739-8529, Japan.
63 25 Key Laboratory of Atmospheric Environment and Extreme Meteorology, Institute of Atmospheric Physics, Chinese
64 Academy of Sciences, Beijing, China.
65 26 Department of Earth, Atmospheric, and Planetary Sciences, Department of Agronomy, Purdue University, West
66 Lafayette, IN, USA.
67 27 Center for Global Environmental Research, National Institute for Environmental Studies, Tsukuba, Ibaraki, Japan.
68 28 Biological Sciences Division, Pacific Northwest National Laboratory, Richland, WA, USA.
69 29 Climate Research Division, Environment and Climate Change Canada, Victoria, BC, Canada.
70 30 Meteorological Research Institute (MRI), Nagamine 1-1, Tsukuba, Ibaraki 305-0052, Japan.
71 31 Sino-French Institute for Earth System Science, College of Urban and Environmental Sciences, Peking University,
72 Beijing 100871, China
73 32 Department of Biology Sciences, University of Quebec at Montreal, C.P. 8888, Succ. Centre-Ville, Montreal, QC H3C
74 3P8, Canada.
75 33 College of Geographic Science, Hunan Normal University, Changsha 410081, China.
76 34 School of Atmospheric Sciences, Sun Yat-sen University, and Southern Marine Science and Engineering Guangdong
77 Laboratory (Zhuhai), Zhuhai 519000, China.
78 35 School of the Environment, Yale University, New Haven, CT, USA.
79 36 Climate and Ecosystem Sciences Division, Lawrence Berkeley National Laboratory, Berkeley, CA, USA.
80 37 TNO, Department of Climate Air & Sustainability, P.O. Box 80015, NL-3508-TA, Utrecht, the Netherlands.
81 38 Finnish Meteorological Institute, P.O. Box 503, 00101, Helsinki, Finland.
82 39 Department of Earth and Atmospheric Sciences, University of Houston, Houston, TX, USA.
83 40 Institute of Environment and Ecology, Tsinghua Shenzhen International Graduate School, Tsinghua University, Shenzhen
84 518055, China.
85 41 State Environmental Protection Key Laboratory of Sources and Control of Air Pollution Complex, Beijing 100084,
86 China.
87 42 College of Hydrology and Water Resources, Hohai University, Nanjing 210098, China.

88
89 *Correspondence to:* Mengze Li (mengze@nus.edu.sg)
90
91
92
93
94

95 **Abstract.** Wetlands are the largest natural source of atmospheric methane (CH₄), yet comprehensive
96 global budgets are typically delayed by years, preventing a timely understanding of CH₄ sources, sinks,
97 and trends. To reduce this delay, we present a model emulator-driven framework and accompanying
98 workflow that enable timely, continuous emission updates using a machine-learning emulator to
99 reconstruct spatially explicit monthly emission fields at 1°x1° resolution. We apply this framework to a
100 global dataset of natural vegetated wetland CH₄ emissions to extend the most recent Global Methane
101 Budget (GMB; Saunio et al., 2025) record that covers the 2000-2020 emissions through 2025. In the
102 test data (~30% of the total dataset), the emulator achieved a global R² of 0.65 ± 0.003 (mean ± 95% CI,
103 hereafter) and an RMSE of 5.49 ± 0.12 × 10⁻³ Tg CH₄/year. The emulator is trained on 35 GMB model
104 estimates, including 22 process-based models and 13 atmospheric inversions, paired with 10 ensemble
105 realizations of 11 gridded climate predictor variables from atmospheric reanalyses. Our results show

Deleted: 30 Department of Physical Geography and Ecosystem Science, Lund University, Solvegatan 12, 223 62, Lund, Sweden. 31...

Deleted: 32

Deleted: 33

Deleted: 34

Deleted: 35

Deleted: 36

Deleted: 37

Deleted: 38

Deleted: 39

Deleted: 40

Deleted: 41

Deleted: 42

Deleted: 43

Deleted: several

Deleted: their

Deleted: and applying the

Deleted: at monthly 1°x1° resolution. We developed a machine-learning...

Deleted: to reconstruct spatially explicit monthly emission fields (

Deleted: =

Deleted: =

Deleted: in test data which is ~30% of the total data).

Deleted: (

Deleted: model estimates

Deleted: inversion estimates)

Deleted: White

Deleted: 2

Formatted: Font colour: Black

Formatted: Normal, Border: Top: (No border), Bottom: (No border), Left: (No border), Right: (No border), Between : (No border), Tab stops: 7.96 cm, Centred + 15.92 cm, Right

34 that the global mean predicted wetland CH₄ emissions for 2021-2025 (157.8 ± 2.4 Tg CH₄/year) are not
35 significantly higher (~ 0.05 Tg CH₄/year) than the 2000-2020 baseline. However, this stability masks a
36 significant hemispheric redistribution of emissions. We detect an increase in Northern Hemisphere
37 (NH) emissions in 2021-2025, with mid- and high-latitudes increasing by 0.76 ± 0.07 and 0.35 ± 0.03
38 Tg CH₄/year, respectively, while the tropics and Southern Hemisphere (SH) extratropics show
39 offsetting negative trends (-0.95 ± 0.19 and -0.11 ± 0.02 Tg CH₄/year, respectively). The predicted
40 emissions are able to capture the low emissions in 2023 in South America linked to El Niño-related
41 drought, as reported by recent studies (Ciais et al., 2026; Quinn et al., 2025). Furthermore, we identify a
42 distinct seasonal amplification of global emission trends that peaks in late boreal summer. This new
43 modeled dataset and operational framework bridge the gap between the latest updated budgets and low-
44 latency monitoring, providing a scalable capacity to frequently update global emission estimates and
45 critical early warnings of regional wetland feedback loops. The data are publicly available at
46 <https://doi.org/10.5281/zenodo.18870108> (Li et al., 2026a).

Deleted: 83

Deleted: 38

Deleted: only marginally

Deleted: a surge

Deleted: (z-score: 2.21)

Deleted: (z-score: 1.01),

Deleted: with z-scores of -2.81 and -0.34

Deleted: Post-2020 growth rates of emission anomalies are a magnitude higher than that in 2000-2025, suggesting an intensification of emission variability.

Deleted: growth peaking

Deleted: 2026

148 1 Introduction

49 Wetlands are the largest natural source of methane (CH₄), a potent greenhouse gas, yet they remain one
50 of the most uncertain components of the global CH₄ budget (Saunois et al., 2025; Zhu et al., 2025).
51 They account for 25-30% of global CH₄ emissions and strongly influence the global carbon cycle
52 (Jackson et al., 2024; Li et al., 2026b; Peng et al., 2022; Saunois et al., 2025; Zhang et al., 2023).
53 Quantifying how wetland CH₄ emissions respond to climate variability is essential for interpreting
54 interannual variability in the global CH₄ budget and for understanding recent atmospheric CH₄ changes
55 (Ciais et al., 2026; Gedney et al., 2019a; Parker et al., 2018; Stavert et al., 2022). Community efforts
56 such as the Global Methane Budget (GMB) synthesize process-based “bottom-up” (BU) models and
57 atmospheric “top-down” (TD) inversions to estimate all CH₄ emission sources and sinks (Saunois et al.,
58 2020, 2025). However, the substantial effort required to assemble these products into a reliable
59 ensemble typically leads to lags of multiple years. For instance, the most recent GMB published in 2025
60 (Saunois et al., 2025) covered the period 2000-2020. Although low-latency estimates exist for some
61 individual models (Quinn et al., 2025), accelerating the assembly of a trustworthy multi-model
62 synthesis would better support timely emission monitoring and evidence-based assessment of mitigation
63 progress.

Deleted: .

65 Wetland CH₄ emissions combine biogeochemical and hydrometeorological controls that regulate CH₄
66 production with oxidation processes within sediments and the water column. Temperature exerts a
67 strong influence on microbial methanogenesis and ecosystem respiration (Knox et al. 2019; Bansal et
68 al., 2023; Li et al., 2025; Yvon-Durocher et al., 2014), whereas soil thermal and free-thaw conditions
69 can modulate growing-season length and cold-season CH₄ dynamics (Hyvärinen et al., 2025; Zona et
70 al., 2016). Hydrology, often summarized by water table depth, soil moisture content, and inundation
71 extent, controls oxygen availability and redox conditions and influences wetland CH₄ production and
72 oxidation (Cui et al., 2024; He et al., 2025; Knox et al., 2021). Precipitation, lateral water transport, and

Deleted: significant

Deleted: trustworthy

Deleted: covers

Deleted: are governed by coupled

Deleted: and

Deleted: in

Deleted: sediment and

Deleted: and transport to the atmosphere.

Deleted: while

Deleted: state

Deleted: , thereby influencing

Deleted: 3

Formatted: Font colour: Black

Formatted: Normal, Border: Top: (No border), Bottom: (No border), Left: (No border), Right: (No border), Between : (No border), Tab stops: 7.96 cm, Centred + 15.92 cm, Right

197 surface energy fluxes jointly constrain water balance through inputs and evapotranspiration (Aalto et al.,
198 2025; Helbig et al., 2020; Tyystjärvi et al., 2024). Furthermore, radiation and vegetation state provide
199 proxies of substrate supply and plant-mediated transport pathways that connect below-ground CH₄
200 production to the atmosphere (Helfter et al., 2022; McNicol et al., 2023).

201
202 Currently, global wetland CH₄ emissions are primarily estimated using two approaches: BU and TD,
203 models. Process-based BU models explicitly simulate the complex biogeochemical mechanisms driven
204 by environmental conditions (Zhang et al., 2025). TD atmospheric inversions estimate surface fluxes by
205 optimising prior emission inventories to match observed atmospheric CH₄ concentrations (Patra et al.,
206 2018). Recent studies have increasingly turned to data-driven machine-learning models. For instance,
207 McNicol et al. (2023) upscaled eddy covariance CH₄ fluxes globally using random forest algorithms;
208 Bernard et al. (2025) introduced a satellite observation-based model to simulate temporal emission
209 variability. These machine-learning approaches offer some advantages, including rapid operational
210 speeds and lower computational costs. However, they are constrained by the sparsity of training data,
211 particularly in the tropics and high latitudes.

212
213 Building on these well-established controls and the advancements in data-driven modeling, we provide
214 a low-latency continuation of the GMB gridded wetland CH₄ emissions by extending monthly
215 emissions from 2000-2020 through 2025 at 1°x1° resolution. Our approach is supported by the fact that
216 many key climate, hydrometeorological and vegetation drivers are routinely updated as global gridded
217 datasets, enabling a practical emulator-based pathway for timely wetland CH₄ emission estimates. In
218 this study, wetlands are defined following the GMB natural vegetated wetland category, excluding
219 lakes, rivers, reservoirs, coastal waters and managed sources (Saunois et al., 2025). We emulate each
220 BU and TD ensemble member from GMB using machine-learning models trained on the 2000-2020
221 GMB wetland emission fields and climate predictor variables (e.g., soil temperature and precipitation)
222 from ERA5 reanalysis to yield spatially explicit monthly emissions for 2000-2025 with uncertainty
223 derived from both GMB ensemble spread (35 runs) and ERA5 monthly reanalysis (10 ensemble
224 members). Using the resulting 2000-2025 wetland CH₄ emission data, we then quantify recent emission
225 changes in 2021-2025 relative to 2000-2020, characterize interannual variability in annual regional and
226 latitudinal emission time series, and diagnose long-term growth rates and their seasonality.

227
228 Our proposed framework and dataset provide a lower-latency, scalable tool for spatially explicit
229 wetland CH₄ emission estimates. It provides support for early-warning diagnostics, attribution of recent
230 atmospheric CH₄ anomalies, and provision of timely priors for atmospheric inversions.
231

Deleted:), while

Deleted: for

Deleted: modeling

Deleted: bottom-up (

Deleted:) models

Deleted: top-down (

Deleted:)

Deleted: (

Deleted: ,

Deleted: , while (

Deleted: ,

Deleted: distinct

Deleted: .

Deleted: This

Deleted: This

Deleted: highly responsive and

Deleted: contemporaneous,

Deleted: 4

Formatted: Font colour: Black

Formatted: Normal, Border: Top: (No border), Bottom: (No border), Left: (No border), Right: (No border), Between : (No border), Tab stops: 7.96 cm, Centred + 15.92 cm, Right

249 2 Methods

250 2.1 Input datasets

251 2.1.1 Wetland CH₄ flux data

252 We used monthly net CH₄ flux estimates for natural vegetated wetlands from the most recent Global
253 Methane Budget (GMB) synthesis for 2000-2020, including both process-based BU models and
254 atmospheric TD inversions (Saunois et al., 2025; Zhang et al., 2025). In this study, the natural vegetated
255 wetland definition excludes lakes, rivers, reservoirs, coastal waters, and managed sources, following the
256 underlying GMB definition (Saunois et al., 2025). Detailed descriptions of each model and inversion
257 framework are provided in the cited GMB publications; here we summarize the key elements relevant to
258 this study.

259 The BU wetland biogeochemical models (22 estimates, Table S1) included in the analysis are from 11
260 models: CLASSIC (Arora et al., 2018; Melton and Arora, 2016), ELM-ECA (Riley et al., 2011), ISAM
261 (Shu et al., 2020; Xu et al., 2021), JSBACH (Kleinen et al., 2020, 2021, 2023), JULES (Gedney et al.,
262 2019b), LPJ-MPI (Kleinen et al., 2012), LPJ-WSL (Zhang et al., 2016), LPX-Bern (Spahni et al., 2011;
263 Stocker et al., 2014), ORCHIDEE (Ringeval et al., 2011), SDGVM (Beerling and Woodward, 2001;
264 Hopcroft et al., 2011, 2020), and VISIT (Ito and Inatomi, 2012). Each model was run under two global
265 climate forcings (CRU and GSWP3-W5E5). All BU simulations are prognostic, i.e. each model
266 computes wetland extent internally rather than relying on a shared wetland extent dataset. Differences in
267 simulated wetland extent therefore contribute to inter-model spread in CH₄ emissions and may explain a
268 substantial fraction of discrepancies across regions.

270 The TD inversion products (13 estimates, Table S2) were constrained by surface or satellite
271 observations over the 2000-2020 period and they are from seven systems: CarbonTracker Europe-CH₄
272 (Tsuruta et al., 2017), LMDz-CIF (Thanwerdas et al., 2022), LMDz-PYVAR (Zheng et al., 2018a, b,
273 2019), MIROC4-ACTM (Chandra et al., 2021; Patra et al., 2018), NISMOM-CH₄ (Niwa et al., 2022,
274 2025), and NIES-TM-FLEXPART (NFVAR) (Maksyutov et al., 2021; Wang et al., 2019). Two
275 alternative anthropogenic prior inventories, EDGAR v6 (Crippa et al., 2021) and GAINS (Höglund-
276 Isaksson et al., 2020), were used to represent anthropogenic emissions. Wetland and inland freshwater
277 emissions were prescribed as separate prior fluxes in the inversion framework. Wetland priors were
278 derived from the ensemble mean of dynamic process-based BU wetland models used in the GMB
279 estimates, whereas inland freshwater emissions were based on independent BU estimates. We used
280 posterior flux estimates throughout this study.

282 All BU and TD outputs provide monthly wetland CH₄ flux as emission per grid cell area, typically at
283 1°x1° resolution in the regridded GMB output products. Coarser products (CLASSIC models at 1.85°
284 and JSBACH models at 2.8°) were remapped to a 1°x1° grid for spatial consistency across datasets. In
285 total, we included 22 BU estimates and 13 TD estimates (35 estimates overall). Tables S1 and S2
286 summarize the BU and TD estimates.

Deleted: wetland

Deleted: ("bottom-up", BU)

Deleted: ("top-down", TD)

Deleted: Each inversion system was driven by two

Deleted: emission

Deleted: (two separate estimates):

Deleted: except NIES-TM-FLEXPART (GOSAT) which was run only under EDGAR v6...

Deleted: prescribed as dynamic emissions

Deleted: 11

Deleted: previous

Deleted: (Saunois et al., 2020).

Deleted: 5

Formatted: Font colour: Black

Formatted: Normal, Border: Top: (No border), Bottom: (No border), Left: (No border), Right: (No border), Between : (No border), Tab stops: 7.96 cm, Centred + 15.92 cm, Right

300

301 2.1.2 Predictor variables from ERA5 reanalysis

302 We assembled 10 ensemble members of global ERA5 monthly averaged data at 0.5° x 0.5° spatial
 303 resolution (Hersbach et al., 2023) for 11 climate predictor variables: t2m (near-surface air temperature),
 304 tp (total precipitation), ssrd (downward shortwave radiation at surface), slhf (surface latent heat flux),
 305 sshf (surface sensible heat flux), swvl1 (volumetric soil water in layers 1, 0-7 cm below surface), swvl2
 306 (volumetric soil water in layers 2, 7-28 cm below surface), stl1 (soil temperature in layer 1, 0-7 cm
 307 below surface), stl2 (soil temperature in layer 2, 7-28 cm below surface), lai_hv (high-vegetation leaf
 308 area index), and lai_lv (low-vegetation leaf area index). LAI (leaf area index) from ERA5 is prescribed
 309 in the ECMWF land-surface model as a seasonally varying, monthly climatology derived from satellite
 310 LAI (Roberts et al., 2018). We chose ERA5 data in part because it is operationally updated regularly,
 311 which enables continuous extension of predictor fields and low-latency updating of emission
 312 reconstructions as new months become available. ERA5 data has also undergone extensive evaluation
 313 and is widely used due to its high spatiotemporal consistency and generally strong performance
 314 (Hersbach et al., 2020), but notably regional biases remain, for example, a weaker performance in parts
 315 of Asia/Africa for hydrology (Gebrechorkos et al., 2024) and temperature in the Arctic (Tian et al.,
 316 2024). The 10 ensemble members correspond to the ERA5 Ensemble of Data Assimilations, which
 317 provides multiple physically consistent realizations of the reanalysis by perturbing the data assimilation
 318 system to sample uncertainty in atmospheric and land-surface states. The ensemble spread can be
 319 interpreted as an indicator of reanalysis uncertainty.

320
 321 The 11 variables included in this analysis represent first-order climatic and biophysical controls on
 322 wetland CH₄ production, oxidation, and transport. Their relevance to wetland CH₄ emissions is well
 323 established in the literature (Knox et al., 2021; Li et al., 2024, 2025; McNicol et al., 2023; Pu et al.,
 324 2024; Toet et al., 2011; Yuan et al., 2022, 2024; Zhang et al., 2025). To represent the ecosystem
 325 memory effect in response to environmental conditions (Chen et al., 2025), we also included 1-month
 326 and 2-month lagged versions of each variable. While introducing short lags would increase collinearity
 327 in the machine-learning model, the risk of overfitting is reduced by our model architecture (Section
 328 2.2.2, including feature screening, regularization, subsampling, and early stopping). The data are
 329 regridded using bilinear interpolation to 1°x1° resolution to match the wetland CH₄ flux data from the
 330 regridded GMB models for further machine-learning modeling.

332 2.2 XGBoost model

333 2.2.1 Data assembly and filtering

334 For each of 350 model-ensemble pairs (35 GMB model estimates x 10 ERA5 ensemble members), we
 335 constructed gridded monthly time series pairing GMB data with a set of 35 predictor variables: 11
 336 contemporaneous ERA5 variables, 22 lagged variables (1- and 2-month lags for each of the 11 ERA5
 337 variables), and two seasonal encoding terms:

6

Deleted: .

Deleted: and their

Moved down [1]: We recognize that many of these variables are multicollinear, an issue that XGBoost is considered robust against. Nevertheless, we minimized overfitting by constraining model complexity (feature screening, regularized trees with subsampling), using a held-out validation window with early stopping to select the optimal number of boosting iterations, and evaluating performance on temporally separated test periods (2000-2002, 2018-2020) not seen during training

Moved down [2]: In addition, using the 10 ERA5 ensemble members allows us to propagate reanalysis uncertainty in the predictor fields through the reconstruction.

Deleted: (see section 2.2.2 Model Architecture).

Deleted: 6

Formatted: Font colour: Black

Formatted: Normal, Border: Top: (No border), Bottom: (No border), Left: (No border), Right: (No border), Between : (No border), Tab stops: 7.96 cm, Centred + 15.92 cm, Right

$$m_{\sin} = \sin(2\pi m/12), m_{\cos} = \cos(2\pi m/12) \quad (\text{Eq.1})$$

Where:

m =month of year (1-12, 1=January and 12=December);

π =the constant pi;

m_{\sin} and m_{\cos} are the sine/cosine transforms of m and represent seasonality.

We optimised our analyses to reduce noise and computational burden by retaining only grid cells with substantial wetland emissions, defined as those maintaining a mean flux of $\geq 10^{-15}$ kg CH₄/m²/s across all GMB model estimates over 2000-2020 (30,000 times lower than the global mean flux).

2.2.2 Model architecture

To systematically reconstruct wetland CH₄ fluxes, we developed a machine-learning pipeline, training independent Extreme Gradient Boosting (XGBoost) models (Chen and Guestrin, 2016) for each grid cell and model-ensemble pair. XGBoost has been applied as a surrogate model for ensemble estimates of GMB BU models with high performance (Zhu et al., 2024). The overall modeling workflow consisted of four stages: (1) data splitting, (2) feature screening, (3) hyperparameter running, and (4) final model fitting and prediction. Each stage is introduced as follows.

Each model-ensemble pair dataset was temporally split into a training set and two testing sets to assess reconstruction capability across different climatic periods at monthly scale. The training data covers January 2003 to December 2017. The testing data covers two periods: January 2000-December 2002 and January 2018-December 2020. Two test windows were used only for out-of-sample evaluation and were not seen during fitting or tuning. The final 24 months of the training period (January 2016 to December 2017) were reserved as a validation set for early stopping and hyperparameter selection. This splitting strategy is to test the model's ability to capture long-term climate variabilities in early/late periods and reduce overfitting.

Prior to XGBoost training, we applied Boruta feature screening (Kursa and Rudnicki, 2010) on the training subset to reduce the effective dimensionality of the predictor set and mitigate overfitting risk arising from the relatively large number of candidate predictors. Boruta augments the predictor matrix with 'shadow' features formed by randomly permuting each predictor across samples, thereby preserving each predictor's marginal distribution while separating its association with CH₄ flux. A random forest regressor is fit to the combined real/shadow feature set and feature importances are compared. Predictor variables were retained if their random forest importance exceeded the maximum shadow-feature importance in more than 20% of 10 iterations (Boruta-style screening), while seasonal terms were always retained. The resulting per-grid cell feature subset was then used for both XGBoost fitting and subsequent reconstructions, ensuring that training and prediction used an identical, cell-specific predictor variable set.

Deleted: mo_sin

Deleted: mo

Deleted: mo_cos

Deleted: mo

Deleted: mo

Deleted: mo_sin

Deleted: mo_cos

Deleted: mo

Deleted: 1×

Deleted: or greater

Formatted: Superscript

Formatted: Superscript

Deleted: an

Deleted: cover

Deleted: cover

Deleted: We implemented an early stopping mechanism using a hold-out validation approach. The last 24 months of the training period were reserved as a validation set (January 2016-December 2017)....

Deleted: 7₁

Formatted: Font colour: Black

Formatted: Normal, Border: Top: (No border), Bottom: (No border), Left: (No border), Right: (No border), Between : (No border), Tab stops: 7.96 cm, Centred + 15.92 cm, Right

409 After the feature screening, we performed a grid search over six hyperparameter configurations
410 (learning rate, maximum tree depth, minimum child weight, subsampling ratio, column subsampling per
411 tree, and L2 regularization) (Table S3). For each configuration, training stopped if the validation Root
412 Mean Squared Error (RMSE) did not improve for 50 consecutive boosting rounds. Once the optimal
413 hyperparameter set was identified for a grid cell, the model was refitted on the full training data using
414 the optimal number of boosting iterations selected during early stopping.

415 After that, the saved booster was then applied to predict wetland CH₄ flux 2000-2025 (including 2021-
416 2025, which extends beyond the most recent GMB estimates period). All the predicted wetland fluxes
417 (unit of kg CH₄/m²/s) were converted to emissions (Tg CH₄/month) by multiplying the fluxes by grid-
418 cell area (m²) and total number of seconds (s) in each month.

420 We recognize that many of these variables are multicollinear, an issue that XGBoost is considered
421 robust against. Nevertheless, we minimized overfitting by constraining model complexity (feature
422 screening, regularized trees with subsampling), using a held-out validation window with early stopping
423 to select the optimal number of boosting iterations, and evaluating performance on temporally separated
424 test periods (2000-2002, 2018-2020) not seen during training. In addition, using the 10 ERA5 ensemble
425 members allows us to propagate reanalysis uncertainty in the predictor fields through the reconstruction.

428 2.2.3 Model evaluation

429 Model performance was evaluated for each grid cell per model-ensemble pair by computing the R²,
430 RMSE, and NRMSE (normalised RMSE, computed by dividing the RMSE by the standard deviation of
431 emissions) values on the withheld test periods. The mean R², RMSE and NRMSE of pairs per grid cell
432 are applied to evaluate model performance at the grid cell level (Figure 1). To assess the model
433 reconstruction skills for grid cells with different emission magnitudes, we grouped grid cells into (1)
434 emission percentile bins based on their total wetland CH₄ emissions during 2000-2020 from GMB
435 estimates, (2) 18 geographical regions, defined in Saunio et al. (2025) (they are USA, Canada, Central
436 America, Northern South America, Brazil, Southwest South America, Europe, Northern Africa,
437 Equatorial Africa, Southern Africa, Russia, Central Asia, Middle East, China, Korea-Japan, South Asia,
438 Southeast Asia, and Australasia), and (3) five latitude bands: global, Northern Hemisphere (NH) high-
439 latitudes (60°N-90°N), NH mid-latitudes (30°N-60°N), tropics (30°N-30°S), and Southern Hemisphere
440 (SH) extratropics (30°S-90°S). We then compared the mean R² and RMSE values of each emission bin
441 (0-10% denotes the highest emitting grid cells) and 18 geographical regions (Figure S1, S2). Monthly
442 mean R² and RMSE at five latitude bands over test periods are presented to study the temporal variation
443 of model performance (Figure S3, S4). Detrended monthly global emissions from GMB and predictions
444 were compared to assess the model performance in capturing interannual variability (Figure S5).
445 Detrended anomalies were calculated by fitting a linear least-squares trend to each monthly time series
446 over 2000-2020 and subtracting the corresponding best-fit linear trend from the original series. We
447 generated out-of-sample wetland CH₄ emission predictions (CH₄_pred) for the test periods to compare

Deleted: Once the optimal hyperparameter combination was identified for a specific grid cell, the model was refitted on the training data using the optimal number of boosting iterations determined during the search. The

Formatted: Superscript

Formatted: Superscript

Moved (insertion) [1]

Deleted: To summarize the mitigation measures for potential overfitting: we (i) use a strict temporal split with training (2003-2017), validation (last 24 months of training) for early stopping, and two disjoint withheld test windows (2000-2002 and 2018-2020), and (ii) constrain model complexity via regularization and subsampling.

Moved (insertion) [2]

Deleted: RMSE

Deleted: ²

Deleted: RMSE

Deleted: , and (3) five latitude bands.

Deleted: 8

Formatted: Font colour: Black

Formatted: Normal, Border: Top: (No border), Bottom: (No border), Left: (No border), Right: (No border), Between : (No border), Tab stops: 7.96 cm, Centred + 15.92 cm, Right

462 with the emissions from GMB models (CH₄_GMB) (Figure 2). This ensured that the model predicted
463 CH₄_pred based on the trained model without having seen the CH₄_GMB in the test data.
464

465 2.3 Emission trend analyses

466 We quantified spatial patterns, regional aggregates and temporal emission trends in reconstructed
467 wetland CH₄ emissions for 2000-2025, and compared them with corresponding GMB estimates over
468 2000-2020. We performed analyses for 18 geographic regions and for five latitude bands.

469
470 We analyzed recent emission changes by comparing 2021-2025 against 2000-2020 baseline at both
471 grid-cell and regional scales (Figures 3, 4). For Figure 3, gridded monthly emissions were aggregated to
472 per-grid mean emissions for each period (2021-2025 and 2000-2020). Emissions presented in Figure 4
473 were summed across grid cells within each region. Emission changes between the two periods were
474 calculated as paired differences for each grid cell and model-ensemble pair. Therefore, the reported
475 mean and 95% confidence interval for emission changes reflect the uncertainty of the paired differences
476 themselves. We examined interannual variability and long-term annual emission changes by
477 aggregating monthly emissions to annual totals for both the latitude bands and 18 geographic regions
478 (Figures 5, S6, S8). Ordinary least squares regression was applied to monthly emissions over 2000-2025
479 to estimate emission trends (Figure 6).

481 2.4 Uncertainty analysis

482 Emulator skill uncertainty was evaluated using held-out test period R², RMSE, NRMSE and prediction
483 residuals relative to the GMB fields (Sections 2.2.3 and 3.1). Uncertainty in reconstructed wetland CH₄
484 emissions was estimated from the ensemble spread across all reconstructions generated from the 35
485 GMB estimates and 10 ERA5 ensemble members. This propagated two sources of uncertainty through
486 the framework: (i) spread in the underlying GMB estimates and (ii) uncertainty in the predictors
487 represented by the ERA5 ensemble. We use 95% confidence interval (CI) to represent this emission
488 uncertainty.

490 3 Results and Discussion

491 3.1 Model performance evaluation

492 We begin by evaluating model performance at the spatial scales most relevant to CH₄ budgeting.
493 Aggregated annual wetland CH₄ emissions at the global and latitudinal-band scales show that the
494 emulator reproduces the overall magnitude, temporal variability, and broad zonal structure of the GMB
495 estimates over 2000-2020 (Figure S6), providing a large-scale context for the finer grid-cell evaluation
496 presented below.

Deleted: defined in Saunio et al., 2025

Deleted: The 18 regions are USA, Canada, Central America, Northern South America, Brazil, Southwest South America, Europe, Northern Africa, Equatorial Africa, Southern Africa, Russia, Central Asia, Middle East, China, Korea-Japan, South Asia, Southeast Asia, and Australasia. Five latitudinal regions are the global, Northern Hemisphere (NH) high latitudes (60°N-90°N), NH mid-latitudes (30°N-60°N), tropics (30°N-30°S), and Southern Hemisphere (SH) extratropics (30°S-90°S).

Deleted: S3, S5

Deleted: 9

Formatted: Font colour: Black

Formatted: Normal, Border: Top: (No border), Bottom: (No border), Left: (No border), Right: (No border), Between : (No border), Tab stops: 7.96 cm, Centred + 15.92 cm, Right

Across the two test windows (2000-2002 and 2018-2020), the XGBoost model reproduces monthly wetland CH₄ emissions well. Globally, the coefficient of determination R² of 0.65 ± 0.003 (mean \pm 95% CI, hereafter; Figure 1a), which refers to the mean grid-cell R² across all global land cells over the two test periods, with the 95% confidence interval calculated across grid cells. This reported reconstructive skill indicates strong predictability from predictor variables. However, the model performance varies geographically. Mean R² is higher in the Southern Hemisphere (SH) than in the Northern Hemisphere (NH) (0.77 ± 0.006 compared with 0.62 ± 0.004 , respectively), and higher in the tropics than in the extratropics (0.78 ± 0.004 and 0.58 ± 0.004 , respectively). In the top emitting regions, mean R² values are generally higher than in regions with lower emissions, (Figure S1a). Global RMSE over test periods is $5.49 \pm 0.12 \times 10^{-3}$ Tg CH₄/year (Figure 1b). RMSE for the tropics is about twice that of the RMSE for the extratropics ($9.37 \pm 0.27 \times 10^{-3}$ and $3.35 \pm 0.08 \times 10^{-3}$ Tg CH₄/year, respectively). Top emitting regions exhibit higher RMSE, e.g., RMSE doubled for top 10% emitting regions compared with top 10-20% emitting regions (Figure S1b). Regionally, mean R² values are highest in Southeast Asia and Korea-Japan (>0.8), and lowest in Russia and Canada (~0.5) (Figure S2a). Mean RMSE is highest in the Americas (Northern South America and Central America), and lowest in the Middle East and Central Asia. Generally, NRMSE is inversely correlated to R², indicating a better performance of our model in top emitting regions (Figure 1c). Temporal variation of model performance reveals the lowest R² in Jan/Feb in NH high latitudes (Figure S3), and the highest RMSE in July-Sep in the tropics (Figure S4). We further evaluate how these spatial and temporal differences in model skill influence long-term variability in annual emissions in Section 3.3.

Deleted: with high skill.

Deleted: is

Deleted: indicating

Deleted: vs

Deleted: Mean

Deleted: is

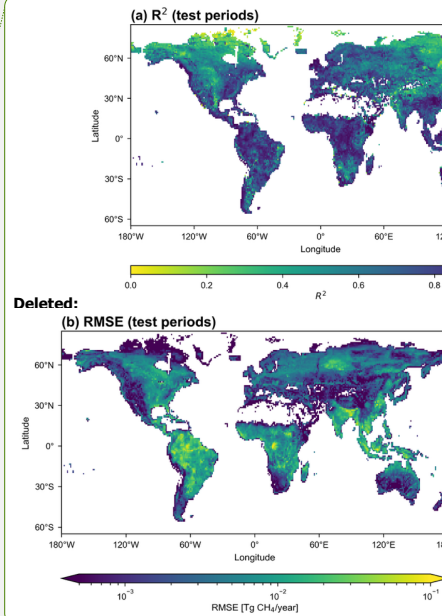
Deleted: higher wetland CH₄

Deleted: ("top emitting regions")

Deleted: At geographical scale

Deleted: is

Deleted: America



Deleted:

Deleted: 10

Formatted: Font colour: Black

Formatted: Normal, Border: Top: (No border), Bottom: (No border), Left: (No border), Right: (No border), Between : (No border), Tab stops: 7.96 cm, Centred + 15.92 cm, Right

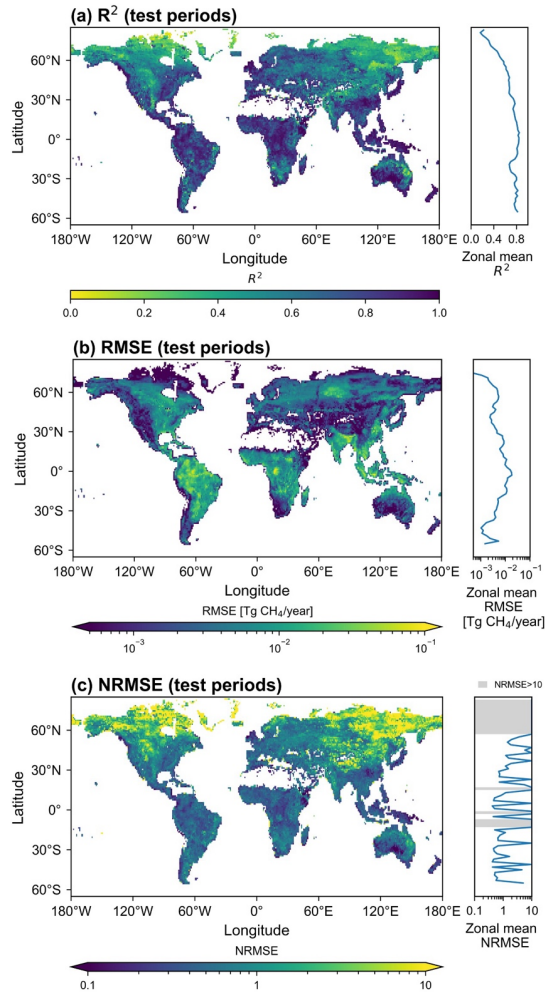


Figure 1. Predictive skill of the XGBoost wetland CH₄ model (per-grid-cell R^2 , RMSE, and NRMSE over the test periods). Insets indicate the zonal mean R^2 , RMSE and NRMSE in 2° latitude bands.

Deleted: RMSE for

Deleted: and

Deleted: ¶

Deleted: ¶¶

Formatted: Font colour: Black

Formatted: Normal, Border: Top: (No border), Bottom: (No border), Left: (No border), Right: (No border), Between : (No border), Tab stops: 7.96 cm, Centred + 15.92 cm, Right

549 To examine predictive uncertainty, we compare wetland CH₄ emissions from the GMB models
550 (CH₄_GMB; Figure 2a) with XGBoost predictions (CH₄_pred; Figure 2b) over the two test periods.
551 Globally, CH₄_pred reproduces both the magnitude and spatial pattern of CH₄_GMB, including the
552 major hotspots concentrated in the tropics, such as Amazon Basin (central-western Amazon floodplains,
553 Pantanal and Moxos plains), Congo Basin, the Sudd wetlands in South Sudan, and Southeast Asia
554 (Sumatra, Borneo, Peninsular Malaysia, and New Guinea), with additional hotspots in NH high
555 latitudes, such as West Siberian Plain and Hudson/James Bay Lowlands.

557 The differences in emissions (Figure 2c) and the corresponding percent emission differences (Figure 2d)
558 between CH₄_GMB and CH₄_pred highlight spatial biases. During the test periods, the global mean
559 predicted wetland CH₄ emission is 158.5 ± 2.1 Tg CH₄/year, which is 2.3 Tg CH₄/year lower than the
560 global mean of CH₄_GMB (160.7 ± 2.2 Tg CH₄/year), corresponding to a 1.4% underestimation (Figure
561 2c). This difference is within the estimated uncertainty range of the two global means. Underestimation
562 is strongest over high-emission systems, such as the central-western Amazon Basin, Southeast Asia,
563 Congo Basin and West Siberian Plain (Figure 2c), where our model predicted emissions are lower than
564 GMB estimates, but percent differences are smaller because the denominator (CH₄_GMB) is large. For
565 example, in Southeast Asia, the mean bias is -0.44 Tg CH₄/year, yet the relative bias is only -1.7%
566 given a high regional mean emission (CH₄_GMB of 25.2 Tg CH₄/year). Monthly anomalies in global
567 emissions reveal small disagreements between the predictions and GMB estimates ($\sim \pm 4$ Tg CH₄/year)
568 (Figure S5). Largest discrepancies occur in July/August 2020 (underestimation of 15 Tg CH₄/year).
569

Deleted: Llanos de

Deleted: (Cuvette Centrale and

Deleted: of

Deleted:),

Deleted: the northern

Deleted: The

Deleted: 27

Deleted: during test periods (Figure 2c

Deleted: 41

Deleted: .

Deleted: absolute emission differences

Deleted: negative

Deleted: 74

Deleted: 23

Deleted: 12

Formatted: Font colour: Black

Formatted: Normal, Border: Top: (No border), Bottom: (No border), Left: (No border), Right: (No border), Between : (No border), Tab stops: 7.96 cm, Centred + 15.92 cm, Right

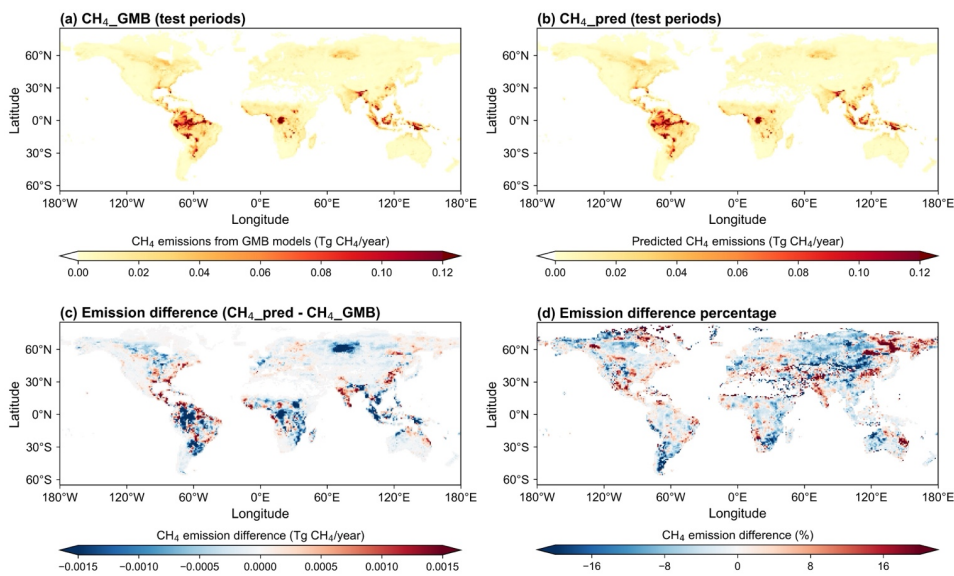


Figure 2. Wetland CH₄ emissions (per 1°x1° grid cell) from GMB models and XGBoost predictions for two test periods combined. (a) Mean CH₄_GMB (GMB emissions) over all test months. (b) Mean CH₄_pred (XGBoost prediction) over all test months. (c) Differences in mean CH₄_GMB and mean CH₄_pred. (d) Percent emission difference between mean CH₄_GMB and mean CH₄_pred. Reds in (c) and (d) indicate higher emissions in CH₄_pred, blues lower emissions.

3.2 Emission trends and predicted anomalies in recent years (2021-2025)

Figure 3 shows spatial maps of global predicted mean wetland CH₄ emissions for 2021-2025 (Figure 3a) and for 2000-2020 (Figure 3b). The 2021-2025 mean emission is 157.8 ± 2.4 Tg CH₄/year ($z=3.72$, with the z -score indicating how far each region's mean emission estimate deviates from the cross-region mean, measured in standard deviation units), representing a non-significant increase of 0.05 Tg CH₄/year relative to the 2000-2020 mean. However, changes are more pronounced across latitudes. NH mid- and high-latitude wetland emissions increase during 2021-2025 by 0.76 ± 0.07 (from 29.9 ± 1.1 in 2000-2020, to 30.7 ± 1.2 in 2021-2025, $z=2.21$) and 0.35 ± 0.03 (from 11.0 ± 0.7 to 11.4 ± 0.7 Tg CH₄/year, $z=1.01$), respectively, compared with 2000-2020 emissions. These changes correspond to ~2.5% and ~0.8% increase. The continued growth in these regions in 2021-2025 (relative to 2000-

Deleted: ¶	... [3]
Formatted	... [4]
Formatted	... [5]
Deleted: 83	
Formatted	... [6]
Deleted: 38	
Formatted	... [7]
Deleted: : 3.72	
Deleted: weak	
Formatted	... [8]
Formatted	... [9]
Deleted: 92	
Deleted: 11(
Formatted	... [10]
Deleted:)	
Deleted: 68	
Deleted: 15 (
Deleted:)) (
Deleted: -score:	
Deleted: 04 ±	
Formatted	... [11]
Formatted	... [12]
Formatted	... [13]
Formatted	... [14]
Formatted	... [15]
Formatted	... [16]
Deleted: .68	
Deleted: 39	
Deleted: 70)	
Formatted	... [17]
Formatted	... [18]
Formatted	... [19]
Formatted	... [20]
Deleted: (
Deleted: -score:	
Formatted	... [21]
Formatted	... [22]
Deleted: 13¶	
Formatted	... [1]
Formatted	... [2]

2020), together with increases reported for 2010-2018 relative to 1981-1989 (Feron et al., 2024), suggests an increasing role of boreal and temperate wetlands in recent decades of global warming. In contrast, emissions decrease in the tropics and SH extratropics during 2021-2025. The tropics exhibit a 0.95 ± 0.19 Tg CH_4 /year emission decrease ($z = -2.81$), from 113.9 ± 2.5 (2000-2020) to 112.9 ± 2.5 Tg CH_4 /year (2021-2025), while SH extratropics emissions decline by 3.5% (-0.11 ± 0.02 Tg CH_4 /year, $z = 0.34$) from 3.1 ± 0.1 (2000-2020) to 3.0 ± 0.1 Tg CH_4 /year (2021-2025).

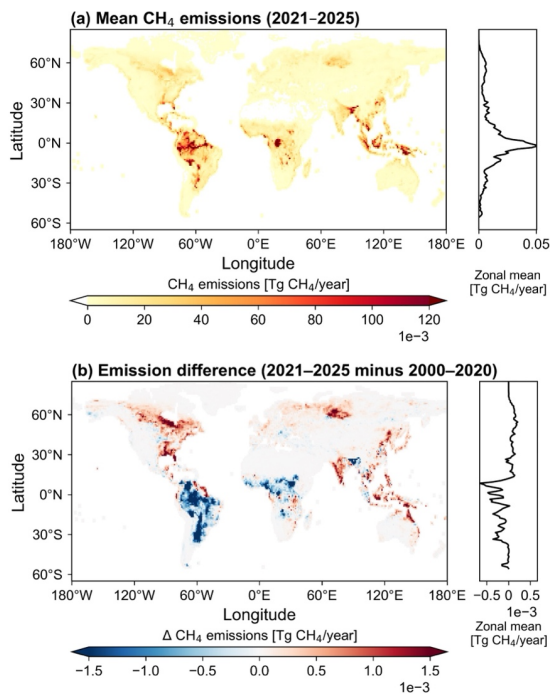


Figure 3. (a) Mean XGBoost model predicted wetland CH_4 emissions for 2021-2025. (b) Difference between mean emissions in 2021-2025 and 2000-2020. Reds indicate higher emissions in 2021-2025, blues lower. Insets indicate the zonal mean in 2° latitude bands.

We further assess regional wetland CH_4 emission changes in 2021-2025 compared with 2000-2020 across 18 regions using XGBoost predictions (Figure 4) across 18 regions. Four regions show no significant change ($p > 0.05$ from two-sided paired significance test, labelled “ns”). Among the 14

Deleted: , this study

Formatted ... [24]

Deleted: -score:-

Deleted: 89

Deleted: 46

Deleted: 94

Deleted: 49

Formatted

Formatted

Formatted

Formatted

Formatted ... [25]

Deleted: -score:-

Deleted: 06

Deleted: 12

Deleted: 2.96 ±

Formatted

Formatted

Formatted

Formatted

Deleted: .12

Formatted ... [26]

(a) Mean CH_4 emissions (2021-2025)

Deleted: ... [27]

Formatted ... [28]

Deleted: ¶ ... [29]

¶ ... [30]

¶ ... [31]

Deleted: 14¶

Formatted: Font colour: Black

Formatted ... [23]

regions with significant changes, nine regions show increases and five show decreases (Northern South America, Brazil, Southwest South America, Northern Africa, and Equatorial Africa). Notably, all regions with decreases are located in South America and Africa. The largest emission changes (2021-2025 relative to 2000-2020) occur in Brazil (-0.59 ± 0.09 Tg CH_4/year), Canada ($+0.46 \pm 0.05$ Tg CH_4/year), Southwest South America (-0.43 ± 0.07 Tg CH_4/year), Russia ($+0.31 \pm 0.03$ Tg CH_4/year), Southeast Asia ($+0.22 \pm 0.03$ Tg CH_4/year) and Equatorial Africa (-0.21 ± 0.04 Tg CH_4/year). The pronounced decline over Brazil possibly reflects the exceptional drought conditions in the Amazon basin during 2022-2024, including record-low river levels and anomalously warm, dry conditions (Espinoza et al., 2024). Such hydroclimatic drying reduces floodplain inundation and lowers water tables, which suppresses anaerobic conditions and thereby limits wetland methane production and emissions (Cui et al., 2024).

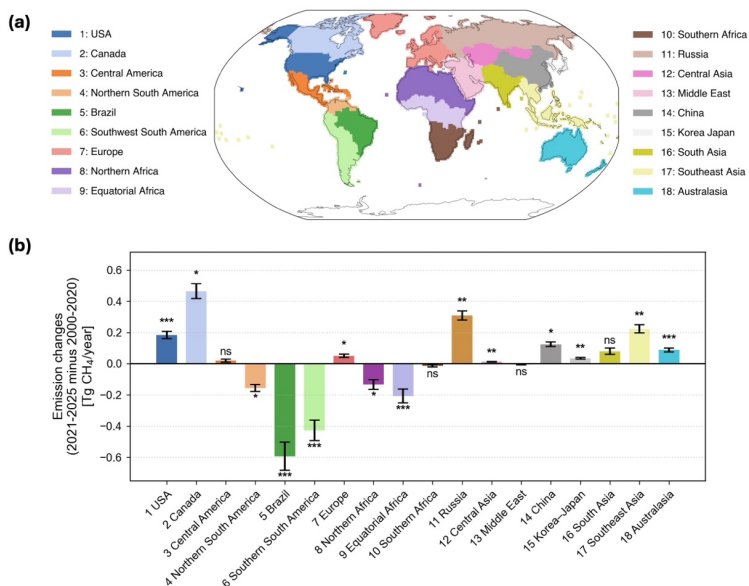
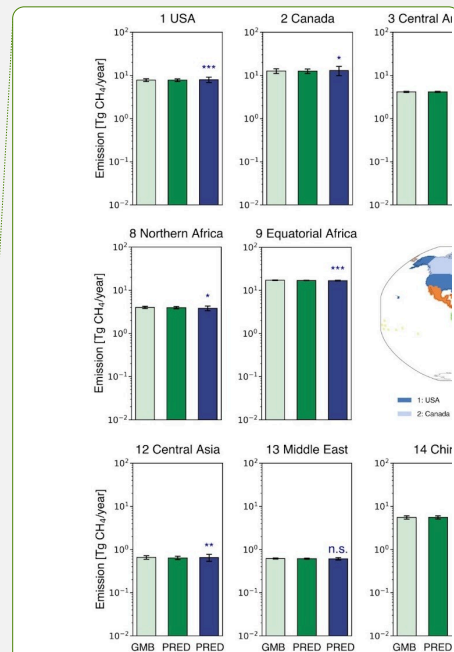


Figure 4. (a) Spatial distribution of the 18 regions; (b) Regional wetland CH_4 emission changes during 2021-2025 relative to 2000-2020 across 18 regions using XGBoost modeled emissions. Bars show regional mean emission changes (annual mean in 2021-2025 minus that in 2000-2020). Error bars indicate 95% CI. A two-sided paired test was applied for each region to assess whether the 2021-2025 mean emission differs from the 2000-2020 mean. Regions with $p \geq 0.05$ are labelled “ns”. Asterisks above bars denote significance: *** for $p < 0.001$, ** for $p < 0.01$, * for $p < 0.05$.



Deleted:

Deleted: emissions for 2000-2020 and

Formatted: Font: 11 pt

Deleted: .

Deleted: emissions: GMB 00-20 (GMB estimates,

Deleted: ; light green), PRED 00-20 (XGBoost predictions, 2000-2020; dark green), PRED 21-25 (XGBoost predictions, 2021-2025; dark blue)....

Deleted: show

Deleted: PRED21-25

Deleted: PRED 00-20

Deleted: n.s.” above the PRED 21-25 bar.

Deleted: PRED 21-25

Deleted: 15

Formatted: Font colour: Black

Formatted: Normal, Border: Top: (No border), Bottom: (No border), Left: (No border), Right: (No border), Between: (No border), Tab stops: 7.96 cm, Centred + 15.92 cm, Right

753 **3.3 26-year emission trends and anomalies (2000-2025)**

754 The emission predictions enable an assessment of long-term trends and interannual variability in
755 wetland emissions over 2000-2025. Annual emission time series show pronounced peaks in 2011 and
756 2016/2017 in the tropics, NH mid-latitudes, and globally (Figure S6). Monthly emission anomalies in
757 these regions (Figure S7) indicate that the annual maxima are driven by sustained positive anomalies
758 during Aug 2010-May 2011 and Aug 2016-Dec 2017, which coincide with La Niña conditions. This
759 alignment is consistent with prior studies reporting La Niña-driven wetting and expanded inundation
760 that enhance tropical wetland CH₄ emissions (Hodson et al., 2011; Lin et al., 2024; Murguia-Flores et
761 al., 2023; Zhang et al., 2020, 2018; Zhu et al., 2017), and with the broader evidence that CH₄ growth in
762 2020-2022 coincided with an unusual persistent La Niña event.

764 In the 2020s, global and tropical annual emissions reach a minimum in 2023 (Figures S6, S7),
765 coincident with a strong El Niño event. This is supported by two recent studies reporting a sharp decline
766 in wetland emissions in South America (Ciais et al., 2026) and Amazonia (Quinn et al., 2025) in 2023
767 linked to El Niño-related drought. Our results further suggest that Brazil and Southern South America
768 are the key contributors, and both rank among the top six emitting regions globally (Figure 5). Annual
769 emissions in Brazil decline steadily across the study period, from 24.8 ± 0.9 Tg CH₄/year in 2000 to
770 23.3 ± 0.9 Tg CH₄/year in 2025, with the lowest emission in 2024 (22.8 ± 0.9 Tg CH₄/year) (Figure 5).
771 Emissions in Southern South America are relatively stable during 2000-2014, decrease markedly during
772 2014-2023 (from 17.2 ± 0.6 to 15.6 ± 0.6 Tg CH₄/year), and show a modest recovery in 2024/2025
773 (Figure 5).

774
775 The remaining four top emitting regions show contrasting behavior. Since 2019, Southeast Asia,
776 Canada and Russia show increasing emissions, whereas Equatorial Africa emissions decrease slightly
777 (Figure 5). Southeast Asian emissions fluctuate around 24.7 ± 0.5 Tg CH₄/year over 2000-2025, with a
778 minimum in 2015 (23.8 ± 0.7 Tg CH₄/year) and a maximum in 2017 (25.6 ± 0.7 Tg CH₄/year).
779 Emissions in Canada are comparatively stable during 2005-2015, while variability is larger before 2005
780 and after 2015: the amplitude reaches ~1.5 Tg CH₄/year in these periods, approximately double that
781 during 2005-2015 (~0.8 Tg CH₄/year). Equatorial African emissions remain 17.0 ± 0.2 Tg CH₄/year
782 during 2000-2025, despite two notable declines during 2002-2005 (-0.5 Tg CH₄/year) and 2019-2025 (-
783 0.6 Tg CH₄/year).

784
785 For regions showing increasing emissions in our XGBoost predictions (e.g., Southeast Asia, Canada,
786 and Russia), these changes are likely driven by wetter and/or warmer conditions that enhance
787 inundation, substrate supply, and CH₄ production. For instance, observed increases in Boreal-Arctic
788 wetland CH₄ emissions have been linked to warming and enhanced ecosystem productivity (Yuan et al.,
789 2024), while inversion-based studies highlight the role of La Niña-driven inundation in enhancing
790 emissions from Equatorial Asia (Qu et al., 2024; Lin et al., 2024; Feng et al., 2022). However, our
791 emulator predictions diverge from recent atmospheric inversion literature regarding African wetland
792 emissions. Multiple top-down studies indicate that enhanced emissions from tropical Africa contributed
793 substantially to the global CH₄ surge during 2020-2024 (Balasus et al., 2026; Qu et al., 2024). In

Deleted:)

Deleted: S3, S4

Deleted: 83

Deleted: 93

Deleted: 28

Deleted: 84

Deleted: 84

Deleted: 85

Deleted: 24

Deleted: 61

Deleted: 95

Deleted: 62

Deleted: -

Deleted: 74

Deleted: 48

Deleted: 75

Deleted: 70

Deleted: 58

Deleted: 73

Deleted: 51

Deleted: 61

Deleted: 16

Formatted: Font colour: Black

Formatted: Normal, Border: Top: (No border), Bottom: (No border), Left: (No border), Right: (No border), Between : (No border), Tab stops: 7.96 cm, Centred + 15.92 cm, Right

contrast, our climate-driven emulator predicts that emissions across Northern, Equatorial, and Southern Africa remained relatively stable or slightly decreased during similar time periods (Figures 4, 5, S8). We attribute this discrepancy to weaker performance and regional precipitation biases of ERA5 data over parts of Africa in capturing complex African hydrological dynamics (Gebrechorkos et al., 2024).

Regional emission time series (Figures 5, S8) help explain the pronounced disagreement in 2019-2020 for global and tropical emissions, where predictions are substantially lower than the GMB estimates (Figure S6). For 2019, the prediction mean emissions are 5.5 Tg CH₄/year below the GMB estimates for global emissions (~3.5% underestimation), while emission changes in Equatorial Africa, Brazil, USA, Southern Africa, and Southern South America jointly account for 4.3 Tg CH₄/year of this discrepancy. In 2020, the modeled mean global emissions are 9.8 Tg CH₄/year lower than GMB (~6% underestimation). The discrepancies in the tropics explain 9.2 Tg CH₄/year of the underestimation, including major regions such as Eastern Africa, Southern South America, Southeast Asia, Brazil, and Northern Africa. Notably, this disagreement in 2019-2020 is not evident in other latitude bands and does not persist outside these years. We cautiously interpret this mismatch as the limitations of the emulator and uncertainty in the underlying GMB ensemble. The climate predictors used in this study can only indirectly capture ENSO (El Niño-Southern Oscillation) effects. Although the training period includes several ENSO events, the unusual persistence of the 2020-2023 triple-dip La Niña may still be underrepresented. In addition, most TD estimates from GMB use a similar prescribed OH (hydroxyl radical) distribution, possibly causing OH-related uncertainty to be underrepresented, particularly during anomalous periods such as COVID.

Deleted: 53

Deleted: 26

Deleted: 84

Deleted: 17

Deleted: 17

Formatted: Font colour: Black

Formatted: Normal, Border: Top: (No border), Bottom: (No border), Left: (No border), Right: (No border), Between : (No border), Tab stops: 7.96 cm, Centred + 15.92 cm, Right

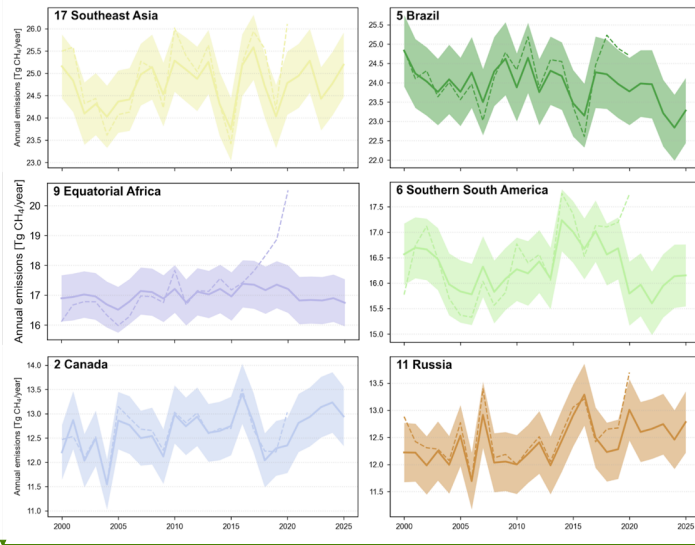
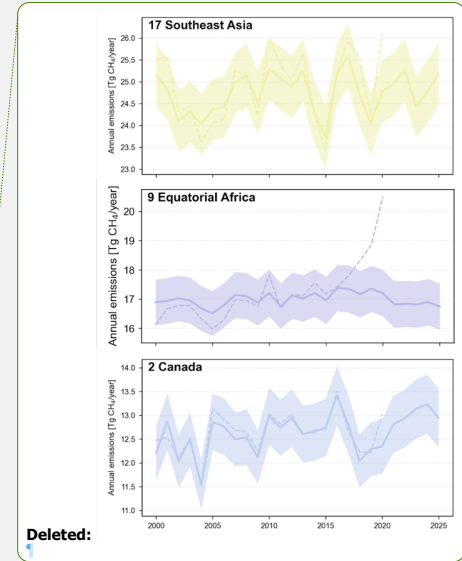


Figure 5. Annual wetland CH₄ emissions for the six top-emitting regions. Solid lines show model predictions of annual mean emissions, and shaded areas indicate 95% CI. Dashed lines show GMB emission estimates (mean). Panel titles indicate the region code and region name, which correspond to the region definitions shown in Figure 4.

Finally, we examine trends in predicted monthly wetland CH₄ emissions across five latitude bands (Figure 6a) and 12 calendar-month categories (Figure 6b). Figure 6a compares these trends across three time periods (2000-2025, 2021-2025, and 2000-2020). Figure 6b shows the trends by 12 calendar-month categories for the 2000-2025 period. We summed predicted monthly emissions across all grid cells within each latitude band to form regional monthly time series, then computed monthly emission anomalies by subtracting the 2000-2025 climatological mean. We then estimated trends (Tg CH₄/year) using ordinary least squares linear regression of the anomaly time series. We calculated a z-score for each region and period by dividing the estimated trend by its standard error to assess the statistical significance of the trends.

The global wetland CH₄ emission trend is three times lower in 2021-2025 compared with the 2000-2020 period (0.05 ± 0.28 and 0.15 ± 0.05 Tg CH₄/year, respectively) (Figure 6a). However, the magnitude of changes in emission trends in NH mid-latitudes, the tropics and SH extratropics is greater in 2021-2025 than 2000-2020 level. Emission trends in NH mid-latitudes increased three times from 0.05 ± 0.02 Tg CH₄/year ($z=4.94$) in 2000-2020 to 0.16 ± 0.12 Tg CH₄/year ($z=2.49$) during 2021-2025. The tropics exhibit a reversal of their emission trends from positive in 2000-2020 (0.07 ± 0.03 Tg CH₄/year,



Deleted:

Deleted: 1 [32]

Deleted: growth rate

Deleted: 2.

Deleted: 89

Deleted: (26 years total, z-score: 4.73)

Deleted: Positive

Deleted: are concentrated

Deleted: the

Deleted: , with the largest increase in the

Deleted: (1.44 ± 0.37 Tg/year, z-score: 7.73) followed by the high-latitudes (0.81 ± 0.24 Tg/year, z-score: 6.70). In contrast,

Deleted: weak

Deleted: 18

Formatted: Font colour: Black

Formatted: Normal, Border: Top: (No border), Bottom: (No border), Left: (No border), Right: (No border), Between : (No border), Tab stops: 7.96 cm, Centred + 15.92 cm, Right

$z=3.95$) to negative in 2021-2025 (-0.18 ± 0.24 Tg CH₄/year, $z=-1.45$). Emission trends in SH extratropics increased from nearly zero in 2000-2020 ($-8.74 \times 10^{-4} \pm 5.18 \times 10^{-3}$ Tg CH₄/year, $z=-0.33$) to higher than the global average in 2021-2025 (0.04 ± 0.02 Tg CH₄/year, $z=3.30$).

Evaluating emission trends over individual months (Figure 6b), we find that the global trend peaks in late boreal summer, with the largest increases in August and September (0.15 ± 0.18 and 0.21 ± 0.13 Tg CH₄/year, respectively). The strongest seasonal intensification occurs in NH mid-latitudes during June-September ($0.09-0.12$ Tg CH₄/year), consistent with the dominant contribution from boreal growing-season emissions. For both NH mid- and high-latitudes, growth rates are systematically higher during May-October (growing season) than during November-April. In the tropics, monthly growth reaches its highest in Oct-Dec and lowest in Jun-Aug (negative growth). SH extratropics show near-zero growth throughout the year (slightly negative).

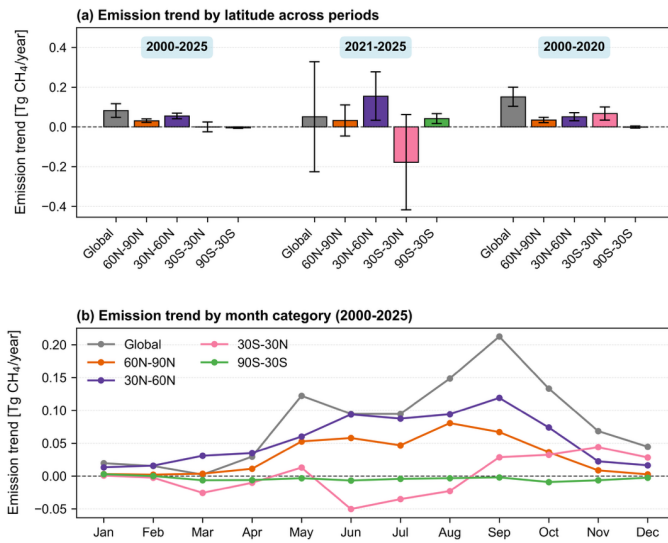
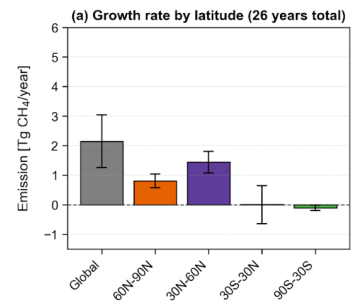


Figure 6. Regional and seasonal trends (Tg CH₄/year) in predicted wetland CH₄ emissions, (a) Trends across five latitude bands across three time periods (2000-2025, 2021-2025, and 2000-2020). (b) Trends for each calendar month over 2000-2025. Positive trends indicate an increase in CH₄ emissions, while negative values indicate a decrease. Error bars indicate 95% CI.

Deleted: growth rates (-
 Deleted: 10
 Deleted: 09
 Deleted: -score: -2.21). The growth rate for the tropics is close to
 Deleted: with higher uncertainty (5.05
 Deleted: ± 0.64
 Deleted: -score: 0.02
 Deleted: growth rates
 Deleted: growth rate
 Deleted: 2.45 ± 2.24
 Deleted: 3.10 ± 1.44
 Deleted: $2.27 - 3.10$



Deleted:

Deleted: growth rates
 Deleted: for 2000-2025.
 Deleted: Growth rates
 Deleted: over the full 26-year period.
 Deleted: Growth rates
 Deleted: across the same period.
 Deleted: growth rates
 Deleted: 19
 Formatted: Font colour: Black
 Formatted: Normal, Border: Top: (No border), Bottom: (No border), Left: (No border), Right: (No border), Between : (No border), Tab stops: 7.96 cm, Centred + 15.92 cm, Right

3.4 Limitation

A limitation concerns source attribution in the TD estimates used for training. Although the TD inversions adopted BU wetland priors that exclude inland freshwater systems, the coarse spatial resolution of TD inversions can still limit the separation of natural vegetated wetland emissions from nearby open-water or inland-freshwater emissions in mixed floodplain environments. This uncertainty cannot be quantified explicitly in the present framework because no independent source-resolved posterior diagnostic is available. Future progress is likely to come from higher-resolution atmospheric inverse frameworks. Two recent studies performed 25 km resolution atmospheric inversions using satellite observations in regional and global applications and improved spatial attribution (East et al., 2025; Hancock et al., 2025).

Another limitation is that our framework predicts wetland emissions from climate predictors only. ENSO-related impacts can be captured only indirectly, while dynamic inundation and atmospheric chemistry perturbations are outside the predictor space of the model.

4 Conclusions

This study presents a framework to extend global natural wetland CH₄ emissions from 2000 through 2025 by applying a machine-learning emulator to provide a lower-latency release of GMB estimates to estimate wetland emissions and is intended for routine updates. The framework reproduces both spatial patterns and interannual variability of the GMB estimates. The extended wetland CH₄ emission record shows that the magnitude of emission changes in 2021-2025 is substantially larger than the long-term trend over 2000-2020, even though the global mean emission change is relatively small.

A key emerging feature is accelerated emissions estimated in the NH mid-latitudes and high-latitudes. Seasonal trend analyses indicate that these increases are concentrated in the warm season (May - Oct), consistent with an amplification of the seasonal cycle and a strengthening of late-summer growth, highlighting Northern mid- and high-latitude wetlands as regions where intensifying trends are most evident in recent years.

In contrast, the tropics show a reversal in emission trend in the post-2020s, from an emission increase during 2000-2020 to a decline in 2021-2025. Nevertheless, the tropics still dominate interannual variability of global wetland emissions and can strongly influence the global CH₄ budget through episodic hydroclimate extremes.

More broadly, this emulator framework may also apply to other low-latency Earth system applications beyond wetland CH₄ emissions, particularly for environments and pollutants that can be constrained by routinely updated predictor fields. At the same time, the present results point to several opportunities for

Formatted: Font colour: Black

Formatted: Border: Top: (No border), Bottom: (No border), Left: (No border), Right: (No border), Between : (No border)

Deleted: disentangle the

Deleted: at low latency, with an operational design

Deleted: relative to 2000-2020

Deleted: 2025

Deleted: extratropics, with the strongest increases in

Deleted: a clear positive signal in

Deleted:

Deleted: ,

Deleted: and SH extratropics

Deleted: weakly negative

Deleted: changes

Deleted: 20

Formatted: Font colour: Black

Formatted: Normal, Border: Top: (No border), Bottom: (No border), Left: (No border), Right: (No border), Between : (No border), Tab stops: 7.96 cm, Centred + 15.92 cm, Right

980 improvement, including better representation of dynamic inundation and improved separation of
981 wetland and inland-freshwater emissions.

982
983 Overall, this work proposes an operational, low-latency emulator framework that provides a scalable
984 pathway to track wetland CH₄ emissions in response to climate anomalies by leveraging routinely
985 updated Earth observation reanalysis data.

986 987 988 989 **Data Availability**

990 ERA5 monthly averaged data are available at Copernicus Climate Change Service Climate Data Store
991 at <https://cds.climate.copernicus.eu/datasets/reanalysis-era5-single-levels-monthly-means?tab=overview>
992 (DOI:10.24381/cds.f17050d7) (Accessed on 22-Jan-2026) (Copernicus Climate Change Service, 2023).
993 The global natural wetland methane emission dataset generated from this study is publicly available at
994 <https://doi.org/10.5281/zenodo.18870108> (Li et al., 2026a).

995 996 **Competing Interests**

997 At least one of the (co-)authors is a member of the editorial board of Earth System Science Data.
998

999 **Financial Support**

1000 This research is supported by the National University of Singapore (NUS) Start-Up Grant. R.J.
1001 acknowledges support from the Gordon and Betty Moore Foundation (Grant GBMF11519 to Stanford
1002 University), the Global Methane Office at the Stanford Doerr School of Sustainability, and the John
1003 Wesley Powell Center for Analysis and Synthesis of the U.S. Geological Survey (“Scaling tropical
1004 wetland methane fluxes regionally and globally” working group). A.M. was supported by an Early
1005 Career Award by the U.S. Department of Energy. F.J. and J.M. acknowledge funding from the Swiss
1006 National Science Foundation (No. 200020_200511). This paper is a contribution to the League of
1007 geophysical research eXcellences for tropical Asia (LeXtra).

1008 1009 1010 **References**

1011 Aalto, T., Tsuruta, A., Mäkelä, J., Müller, J., Tenkanen, M., Burke, E., Chadburn, S., Gao, Y., Mannisenaho, V., Kleinen, T.,
1012 Lee, H., Leppänen, A., Markkanen, T., Matera, S., Miller, P. A., Peano, D., Peltola, O., Poulter, B., Raivonen, M., Saunio,
1013 M., Wärilind, D., and Zaehle, S.: Air temperature and precipitation constraining the modelled wetland methane emissions in a
1014 boreal region in northern Europe, *Biogeosciences*, 22, 323–340, <https://doi.org/10.5194/bg-22-323-2025>, 2025.

Deleted: are

Deleted: 2026

Moved down [3]: A.M. was supported by an Early Career Award by the U.S. Department of Energy. F.J. and J.M. acknowledge funding from the Swiss National Science Foundation (No. 200020_200511). Additional support was provided by

Deleted: Additional support was provided by

Moved (insertion) [3]

Formatted: Font colour: Black

Formatted: Normal, Space Before: 14 pt, After: 14 pt, Border: Top: (No border), Bottom: (No border), Left: (No border), Right: (No border), Between : (No border)

Deleted: 21

Formatted: Font colour: Black

Formatted: Normal, Border: Top: (No border), Bottom: (No border), Left: (No border), Right: (No border), Between : (No border), Tab stops: 7.96 cm, Centred + 15.92 cm, Right

1022 Arora, V. K., Melton, J. R., and Plummer, D.: An assessment of natural methane fluxes simulated by the CLASS-CTEM
1023 model, *Biogeosciences*, 15, 4683–4709, <https://doi.org/10.5194/bg-15-4683-2018>, 2018.

1024 [Balasus, N., Jacob, D. J., Bloom, A. A., East, J. D., Estrada, L. A., Hancock, S. E., He, M., Mooring, T. A., Turner, A. J.,
1025 and Worden, J. R.: 2019–2024 trends in African livestock and wetland emissions as contributors to the global methane rise,
1026 *Atmospheric Chem. Phys.*, 26, 4601–4617, <https://doi.org/10.5194/acp-26-4601-2026>, 2026.](#)

1027 Bansal, S., Post van der Burg, M., Fern, R. R., Jones, J. W., Lo, R., McKenna, O. P., Tangen, B. A., Zhang, Z., and Gleason,
1028 R. A.: Large increases in methane emissions expected from North America’s largest wetland complex, *Sci. Adv.*, 9,
1029 eade1112, <https://doi.org/10.1126/sciadv.ade1112>, 2023.

1030 Beerling, D. and Woodward, F. I.: *Vegetation and the Terrestrial Carbon Cycle: The First 400 Million Years*, Cambridge
1031 University Press, Cambridge, U.K. ; New York, NY, 416 pp., 2001.

1032 Bernard, J., Salmon, E., Saunio, M., Peng, S., Serrano-Ortiz, P., Berchet, A., Gnanamoorthy, P., Jansen, J., and Ciaia, P.:
1033 Satellite-based modeling of wetland methane emissions on a global scale (SatWetCH4 1.0), *Geosci. Model Dev.*, 18, 863–
1034 883, <https://doi.org/10.5194/gmd-18-863-2025>, 2025.

1035 Chandra, N., Patra, P. K., Bisht, J. S. H., Ito, A., Umezawa, T., Saigusa, N., Morimoto, S., Aoki, S., Janssens-Maenhout, G.,
1036 Fujita, R., Takigawa, M., Watanabe, S., Saitoh, N., and Canadell, J. G.: Emissions from the Oil and Gas Sectors, Coal
1037 Mining and Ruminant Farming Drive Methane Growth over the Past Three Decades, *J. Meteorol. Soc. Jpn. Ser II*, 99, 309–
1038 337, <https://doi.org/10.2151/jmsj.2021-015>, 2021.

1039 [Chen, T. and Guestrin, C.: XGBoost: A Scalable Tree Boosting System, in: Proceedings of the 22nd ACM SIGKDD
1040 International Conference on Knowledge Discovery and Data Mining, arXiv:1603.02754 \[cs\], 785–794,
1041 <https://doi.org/10.1145/2939672.2939785>, 2016.](#)

1042 Ciaia, P., Zhu, Y., Cai, Y., Lan, X., Michel, S. E., Zheng, B., Zhao, Y., Hauglustaine, D. A., Lin, X., Zhang, Y., Sun, S.,
1043 Tian, X., Zhao, M., Wang, Y., Chang, J., Dou, X., Liu, Z., Andrew, R., Quinn, C. A., Poulter, B., Ouyang, Z., Yuan, W.,
1044 Yuan, K., Zhu, Q., Li, F., Pan, N., Tian, H., Yu, X., Rocher-Ros, G., Johnson, M. S., Li, M., Li, M., Feng, D., Raymond, P.,
1045 Yang, X., Canadell, J. G., Jackson, R. B., Yu, X., Li, Y., Saunio, M., Bousquet, P., and Peng, S.: Why methane surged in
1046 the atmosphere during the early 2020s, *Science*, 391, eadx8262, <https://doi.org/10.1126/science.adx8262>, 2026.

1047 Copernicus Climate Change Service: ERA5 monthly averaged data on single levels from 1940 to present, Copernicus
1048 Climate Change Service (C3S) Climate Data Store (CDS) [data set]. DOI: 10.24381/cds.fl7050d7 (Accessed on 22-Jan-
1049 2026), 2023.

1050 Crippa, M., Guizzardi, D., Pagani, F., Banja, M., Muntean, M., Schaaf, E., Becker, W., Monforti-Ferrario, F., Quadrelli, R.,
1051 and Risquez Martin, A.: GHG emissions of all world countries– 2021 Report, Publ. Off. Eur. Union Luxemb., 2021.

1052 Cui, S., Liu, P., Guo, H., Nielsen, C. K., Pullens, J. W. M., Chen, Q., Pugliese, L., and Wu, S.: Wetland hydrological
1053 dynamics and methane emissions, *Commun. Earth Environ.*, 5, 470, <https://doi.org/10.1038/s43247-024-01635-w>, 2024.

1054 [East, J. D., Jacob, D. J., Jervis, D., Balasus, N., Estrada, L. A., Hancock, S. E., Sulprizio, M. P., Thomas, J., Wang, X., Chen,
1055 Z., Varon, D. J., and Worden, J. R.: Worldwide inference of national methane emissions by inversion of satellite
1056 observations with UNFCCC prior estimates, *Nat. Commun.*, 16, 11004, <https://doi.org/10.1038/s41467-025-67122-8>, 2025.](#)

Formatted: Font colour: Black

Formatted: Normal, Space Before: 14 pt, After: 14 pt,
Border: Top: (No border), Bottom: (No border), Left: (No
border), Right: (No border), Between : (No border)

Formatted: Font colour: Black

Formatted: Normal, Space Before: 14 pt, After: 14 pt,
Border: Top: (No border), Bottom: (No border), Left: (No
border), Right: (No border), Between : (No border)

Deleted: 22

Formatted: Font colour: Black

Formatted: Normal, Border: Top: (No border), Bottom: (No
border), Left: (No border), Right: (No border), Between : (No
border), Tab stops: 7.96 cm, Centred + 15.92 cm, Right

1057 Espinoza, J.-C., Jimenez, J. C., Marengo, J. A., Schongart, J., Ronchail, J., Lavado-Casimiro, W., and Ribeiro, J. V. M.: The
1058 new record of drought and warmth in the Amazon in 2023 related to regional and global climatic features, *Sci. Rep.*, 14,
1059 8107, <https://doi.org/10.1038/s41598-024-58782-5>, 2024.

1060 Feng, L., Palmer, P. I., Zhu, S., Parker, R. J., and Liu, Y.: Tropical methane emissions explain large fraction of recent
1061 changes in global atmospheric methane growth rate, *Nat. Commun.*, 13, 1378, <https://doi.org/10.1038/s41467-022-28989-z>,
1062 2022.

1063 Feron, S., Malhotra, A., Bansal, S., Fluet-Chouinard, E., McNicol, G., Knox, S. H., Delwiche, K. B., Cordero, R. R.,
1064 Ouyang, Z., Zhang, Z., Poulter, B., and Jackson, R. B.: Recent increases in annual, seasonal, and extreme methane fluxes
1065 driven by changes in climate and vegetation in boreal and temperate wetland ecosystems, *Glob. Change Biol.*, 30, e17131,
1066 <https://doi.org/10.1111/gcb.17131>, 2024.

1067 Gebrechorkos, S. H., Leyland, J., Dadson, S. J., Cohen, S., Slater, L., Wortmann, M., Ashworth, P. J., Bennett, G. L.,
1068 Boothroyd, R., Cloke, H., Delorme, P., Griffith, H., Hardy, R., Hawker, L., McLelland, S., Neal, J., Nicholas, A., Tatem, A.
1069 J., Vahidi, E., Liu, Y., Sheffield, J., Parsons, D. R., and Darby, S. E.: Global-scale evaluation of precipitation datasets for
1070 hydrological modelling, *Hydrol. Earth Syst. Sci.*, 28, 3099–3118, <https://doi.org/10.5194/hess-28-3099-2024>, 2024.

1071 Gedney, N., Huntingford, C., Comyn-Platt, E., and Wiltshire, A.: Significant feedbacks of wetland methane release on
1072 climate change and the causes of their uncertainty, *Environ. Res. Lett.*, 14, 084027, <https://doi.org/10.1088/1748-9326/ab2726>, 2019a.

1074 Gedney, N., Huntingford, C., Comyn-Platt, E., and Wiltshire, A.: Significant feedbacks of wetland methane release on
1075 climate change and the causes of their uncertainty, *Environ. Res. Lett.*, 14, 084027, <https://doi.org/10.1088/1748-9326/ab2726>, 2019b.

1077 Hancock, S. E., Jacob, D. J., Chen, Z., Nesser, H., Davitt, A., Varon, D. J., Sulprizio, M. P., Balasus, N., Estrada, L. A.,
1078 Cazorla, M., Dawidowski, L., Diez, S., East, J. D., Penn, E., Randles, C. A., Worden, J., Aben, I., Parker, R. J., and
1079 Maasakkers, J. D.: Satellite quantification of methane emissions from South American countries: a high-resolution inversion
1080 of TROPOMI and GOSAT observations, *Atmospheric Chem. Phys.*, 25, 797–817, <https://doi.org/10.5194/acp-25-797-2025>,
1081 2025.

1082 Hasan, N. A., Chikamoto, Y., and McPhaden, M. J.: The influence of tropical basin interactions on the 2020–2022 double-
1083 dip La Niña, *Front. Clim.*, 4, <https://doi.org/10.3389/fclim.2022.1001174>, 2022.

1084 He, K., Li, W., Zhang, Y., Zeng, A., de Graaf, I. E. M., Aguilós, M., Sun, G., McNulty, S. G., King, J. S., Flanagan, N. E.,
1085 and Richardson, C. J.: Temperature and Water Levels Collectively Regulate Methane Emissions From Subtropical
1086 Freshwater Wetlands, *Glob. Biogeochem. Cycles*, 39, e2024GB008372, <https://doi.org/10.1029/2024GB008372>, 2025.

1087 Helbig, M., Waddington, J. M., Alekseychik, P., Amiro, B. D., Aurela, M., Barr, A. G., Black, T. A., Blanken, P. D., Carey,
1088 S. K., Chen, J., Chi, J., Desai, A. R., Dunn, A., Euskirchen, E. S., Flanagan, L. B., Forbrich, I., Friborg, T., Grelle, A.,
1089 Harder, S., Heliasz, M., Humphreys, E. R., Ikawa, H., Isabelle, P.-E., Iwata, H., Jassal, R., Korkiakoski, M., Kurbatova, J.,
1090 Kutzbach, L., Lindroth, A., Löfvenius, M. O., Lohila, A., Mammarella, I., Marsh, P., Maximov, T., Melton, J. R., Moore, P.
1091 A., Nadeau, D. F., Nicholls, E. M., Nilsson, M. B., Ohta, T., Peichl, M., Petrone, R. M., Petrov, R., Prokushkin, A., Quinton,
1092 W. L., Reed, D. E., Roulet, N. T., Runkle, B. R. K., Sonnentag, O., Strachan, I. B., Taillardat, P., Tuittila, E.-S., Tuovinen,
1093 J.-P., Turner, J., Ueyama, M., Varlagin, A., Wilmking, M., Wofsy, S. C., and Zyryanov, V.: Increasing contribution of
1094 peatlands to boreal evapotranspiration in a warming climate, *Nat. Clim. Change*, 10, 555–560,
1095 <https://doi.org/10.1038/s41558-020-0763-7>, 2020.

Formatted: Font colour: Black

Formatted: Normal, Space Before: 14 pt, After: 14 pt,
Border: Top: (No border), Bottom: (No border), Left: (No
border), Right: (No border), Between : (No border)

Formatted: Font colour: Black

Formatted: Normal, Space Before: 14 pt, After: 14 pt,
Border: Top: (No border), Bottom: (No border), Left: (No
border), Right: (No border), Between : (No border)

Formatted: Font colour: Black

Formatted: Normal, Space Before: 14 pt, After: 14 pt,
Border: Top: (No border), Bottom: (No border), Left: (No
border), Right: (No border), Between : (No border)

Deleted: 23

Formatted: Font colour: Black

Formatted: Normal, Border: Top: (No border), Bottom: (No
border), Left: (No border), Right: (No border), Between : (No
border), Tab stops: 7.96 cm, Centred + 15.92 cm, Right

1096 Helfter, C., Gondwe, M., Murray-Hudson, M., Makati, A., Lunt, M. F., Palmer, P. I., and Skiba, U.: Phenology is the
1097 dominant control of methane emissions in a tropical non-forested wetland, *Nat. Commun.*, 13, 133,
1098 <https://doi.org/10.1038/s41467-021-27786-4>, 2022.

1099 Hersbach, H., Bell, B., Berrisford, P., Hirahara, S., Horányi, A., Muñoz-Sabater, J., Nicolas, J., Peubey, C., Radu, R.,
1100 Schepers, D., Simmons, A., Soci, C., Abdalla, S., Abellan, X., Balsamo, G., Bechtold, P., Biavati, G., Bidlot, J., Bonavita,
1101 M., De Chiara, G., Dahlgren, P., Dee, D., Diamantakis, M., Dragani, R., Flemming, J., Forbes, R., Fuentes, M., Geer, A.,
1102 Haimberger, L., Healy, S., Hogan, R. J., Hólm, E., Janisková, M., Keeley, S., Laloyaux, P., Lopez, P., Lupu, C., Radnoti, G.,
1103 de Rosnay, P., Rozum, I., Vamborg, F., Villaume, S., and Thépaut, J.-N.: The ERA5 global reanalysis, *Q. J. R. Meteorol.*
1104 *Soc.*, 146, 1999–2049, <https://doi.org/10.1002/qj.3803>, 2020.

1105 Hersbach, H., Bell, B., Berrisford, P., Biavati, G., Horányi, A., Muñoz Sabater, J., Nicolas, J., Peubey, C., Radu, R., and
1106 Rozum, I.: ERA5 monthly averaged data on pressure levels from 1940 to present, Copernicus Climate Change Service (C3S)
1107 Climate Data Store (CDS)[data set], 2023.

1108 Höglund-Isaksson, L., Gómez-Sanabria, A., Klimont, Z., Rafaj, P., and Schöpp, W.: Technical potentials and costs for
1109 reducing global anthropogenic methane emissions in the 2050 timeframe –results from the GAINS model, *Environ. Res.*
1110 *Commun.*, 2, 025004, <https://doi.org/10.1088/2515-7620/ab7457>, 2020.

1111 Hopcroft, P. O., Valdes, P. J., and Beerling, D. J.: Simulating idealized Dansgaard-Oeschger events and their potential
1112 impacts on the global methane cycle, *Quat. Sci. Rev.*, 30, 3258–3268, <https://doi.org/10.1016/j.quascirev.2011.08.012>, 2011.

1113 Hopcroft, P. O., Ramstein, G., Pugh, T. A. M., Hunter, S. J., Murguía-Flores, F., Quiquet, A., Sun, Y., Tan, N., and Valdes,
1114 P. J.: Polar amplification of Pliocene climate by elevated trace gas radiative forcing, *Proc. Natl. Acad. Sci.*, 117, 23401–
1115 23407, <https://doi.org/10.1073/pnas.2002320117>, 2020.

1116 Hyvärinen, S., Tenkanen, M. K., Tsuruta, A., Erkkilä, A., Rautiainen, K., Aaltonen, H., Sasakawa, M., and Aalto, T.: Spring
1117 melting season methane emissions in northern high latitude wetlands are governed by the length of the season and presence
1118 of permafrost, *EGUsphere*, 1–46, <https://doi.org/10.5194/egusphere-2025-2794>, 2025.

1119 Ito, A. and Inatomi, M.: Use of a process-based model for assessing the methane budgets of global terrestrial ecosystems and
1120 evaluation of uncertainty, *Biogeosciences*, 9, 759–773, <https://doi.org/10.5194/bg-9-759-2012>, 2012.

1121 Jackson, R. B., Saunio, M., Martinez, A., Canadell, J. G., Yu, X., Li, M., Poulter, B., Raymond, P. A., Regnier, P., Ciais, P.,
1122 Davis, S. J., and Patra, P. K.: Human activities now fuel two-thirds of global methane emissions, *Environ. Res. Lett.*, 19,
1123 101002, <https://doi.org/10.1088/1748-9326/ad6463>, 2024.

1124 Kleinen, T., Brovkin, V., and Schuldt, R. J.: A dynamic model of wetland extent and peat accumulation: results for the
1125 Holocene, *Biogeosciences*, 9, 235–248, <https://doi.org/10.5194/bg-9-235-2012>, 2012.

1126 Kleinen, T., Mikolajewicz, U., and Brovkin, V.: Terrestrial methane emissions from the Last Glacial Maximum to the
1127 preindustrial period, *Clim. Past*, 16, 575–595, <https://doi.org/10.5194/cp-16-575-2020>, 2020.

1128 Kleinen, T., Gromov, S., Steil, B., and Brovkin, V.: Atmospheric methane underestimated in future climate projections,
1129 *Environ. Res. Lett.*, 16, 094006, <https://doi.org/10.1088/1748-9326/ac1814>, 2021.

1130 Kleinen, T., Gromov, S., Steil, B., and Brovkin, V.: Atmospheric methane since the last glacial maximum was driven by
1131 wetland sources, *Clim. Past*, 19, 1081–1099, <https://doi.org/10.5194/cp-19-1081-2023>, 2023.

Deleted: 24

Formatted: Font colour: Black

Formatted: Normal, Border: Top: (No border), Bottom: (No border), Left: (No border), Right: (No border), Between : (No border), Tab stops: 7.96 cm, Centred + 15.92 cm, Right

1132 Knox, S. H., Bansal, S., McNicol, G., Schafer, K., Sturtevant, C., Ueyama, M., Valach, A. C., Baldocchi, D., Delwiche, K.,
1133 Desai, A. R., Euskirchen, E., Liu, J., Lohila, A., Malhotra, A., Melling, L., Riley, W., Runkle, B. R. K., Turner, J., Vargas,
1134 R., Zhu, Q., Alto, T., Fluet-Chouinard, E., Goeckede, M., Melton, J. R., Sonnentag, O., Vesala, T., Ward, E., Zhang, Z.,
1135 Feron, S., Ouyang, Z., Alekseychik, P., Aurela, M., Bohrer, G., Campbell, D. I., Chen, J., Chu, H., Dalmagro, H. J.,
1136 Goodrich, J. P., Gottschalk, P., Hirano, T., Iwata, H., Jurasinski, G., Kang, M., Koebsch, F., Mammarella, I., Nilsson, M. B.,
1137 Ono, K., Peichl, M., Peltola, O., Ryu, Y., Sachs, T., Sakabe, A., Sparks, J. P., Tuittila, E.-S., Vourlitis, G. L., Wong, G. X.,
1138 Windham-Myers, L., Poulter, B., and Jackson, R. B.: Identifying dominant environmental predictors of freshwater wetland
1139 methane fluxes across diurnal to seasonal time scales, *Glob. Change Biol.*, 27, 3582–3604,
1140 <https://doi.org/10.1111/gcb.15661>, 2021.

1141 [Knox, S. H., Jackson, R. B., Poulter, B., McNicol, G., Fluet-Chouinard, E., Zhang, Z., Hugelius, G., Bousquet, P., Canadell,](#)
1142 [J. G., Saunio, M., Papale, D., Chu, H., Keenan, T. F., Baldocchi, D., Torn, M. S., Mammarella, I., Trotta, C., Aurela, M.,](#)
1143 [Bohrer, G., Campbell, D. I., Cescatti, A., Chamberlain, S., Chen, J., Chen, W., Dengel, S., Desai, A. R., Euskirchen, E.,](#)
1144 [Friborg, T., Gasbarra, D., Godeed, I., Goeckede, M., Heimann, M., Helbig, M., Hirano, T., Hollinger, D. Y., Iwata, H., Kang,](#)
1145 [M., Klatt, J., Krauss, K. W., Kutzbach, L., Lohila, A., Mitra, B., Morin, T. H., Nilsson, M. B., Niu, S., Noormets, A., Oechel,](#)
1146 [W. C., Peichl, M., Peltola, O., Reba, M. L., Richardson, A. D., Runkle, B. R. K., Ryu, Y., Sachs, T., Schäfer, K. V. R.,](#)
1147 [Schmid, H. P., Shurpali, N., Sonnentag, O., Tang, A. C. I., Ueyama, M., Vargas, R., Vesala, T., Ward, E. J., Windham-](#)
1148 [Myers, L., Wohlfahrt, G., and Zona, D.: FLUXNET-CH4 Synthesis Activity: Objectives, Observations, and Future](#)
[Directions](https://doi.org/10.1175/BAMS-D-18-0268.1), <https://doi.org/10.1175/BAMS-D-18-0268.1>, 2019.

1150 [Kursa, M. B. and Rudnicki, W. R.: Feature Selection with the Boruta Package](#), *J. Stat. Softw.*, 36, 1–13,
1151 <https://doi.org/10.18637/jss.v036.i11>, 2010.

1152 [Li, F., Zhu, Q., Yuan, K., Fluet-Chouinard, E., Zhang, X., Wang, J., Knox, S. H., You, H., Chen, M., Li, M., Stern, R., Hoyt,](#)
1153 [A. M., McNicol, G., Riley, W. J., Peng, S., Poulter, B., Malhotra, A., Cooley, S., Zhang, Z., Hong, S., Chen, Z., Zhu, Z.,](#)
1154 [Raymond, P. A., Ciais, P., and Jackson, R. B.: The underappreciated importance of small wetlands in global methane](#)
1155 [emissions](#), *Nat. Clim. Change*, 1–5, <https://doi.org/10.1038/s41558-026-02609-w>, 2026b.

1156 [Li, M., Jackson, R. B., Saunio, M., Ciais, P., Poulter, B., Canadell, J. G., Patra, P. K., Tian, H., Zhang, Z., Fluet-Chouinard,](#)
1157 [E., Ouyang, Z., Zhang, T., Beerling, D. J., Belikov, D. A., Bousquet, P., Custodio, D., Chandra, N., Dou, X., Gedney, N.,](#)
1158 [Hopcroft, P. O., Hoyt, A. M., Ichii, K., Ito, A., Jain, A. K., Jensen, K., Joos, F., Kleinen, T., Kondo, M., Li, F., Li, T., Liu,](#)
1159 [X., Maksyutov, S., Malhotra, A., Martinez, A., McDonald, K., Melton, J. R., Miller, P., Müller, J., Niwa, Y., Pan, S., Peng,](#)
1160 [S., Peng, C., Qin, Z., Raymond, P., Riley, W., Segers, A., Thompson, R. L., Tsuruta, A., Yi, X., Yuan, K., Zhang, W.,](#)
1161 [Zheng, B., Zhu, Q., Zhu, Q., and Zhuang, Q.: Global natural wetland methane emissions \(2000–2025\) \(Version v1\), Zenodo](#)
1162 [\[data set\]](https://doi.org/10.5281/zenodo.18870109), <https://doi.org/10.5281/zenodo.18870109>, 2026a.

1163 [Li, M., Kort, E. A., Bloom, A. A., Wu, D., Plant, G., Gerlein-Safdi, C., and Pu, T.: Underestimated Dry Season Methane](#)
1164 [Emissions from Wetlands in the Pantanal](#), *Environ. Sci. Technol.*, 58, 3278–3287, <https://doi.org/10.1021/acs.est.3c09250>,
1165 2024.

1166 [Li, M., Li, F., Malhotra, A., Knox, S. H., Stern, R., and Jackson, R. B.: Key Environmental and Ecological Variables of](#)
1167 [Wetland CH4 and CO2 Fluxes Change With Warming](#), *Earths Future*, 13, e2024EF005751,
1168 <https://doi.org/10.1029/2024EF005751>, 2025.

1169 [Lin, X., Peng, S., Ciais, P., Hauglustaine, D., Lan, X., Liu, G., Ramonet, M., Xi, Y., Yin, Y., Zhang, Z., Bösch, H.,](#)
1170 [Bousquet, P., Chevallier, F., Dong, B., Gerlein-Safdi, C., Halder, S., Parker, R. J., Poulter, B., Pu, T., Remaud, M., Runge,](#)
1171 [A., Saunio, M., Thompson, R. L., Yoshida, Y., and Zheng, B.: Recent methane surges reveal heightened emissions from](#)
1172 [tropical inundated areas](#), *Nat. Commun.*, 15, 10894, <https://doi.org/10.1038/s41467-024-55266-y>, 2024.

Formatted: Font colour: Black

Formatted: Normal, Space Before: 14 pt, After: 14 pt,
Border: Top: (No border), Bottom: (No border), Left: (No
border), Right: (No border), Between : (No border)

Formatted: Font colour: Black

Formatted: Normal, Space Before: 14 pt, After: 14 pt,
Border: Top: (No border), Bottom: (No border), Left: (No
border), Right: (No border), Between : (No border)

Deleted: 2026

Formatted: Font colour: Black

Deleted: 25

Formatted: Font colour: Black

Formatted: Normal, Border: Top: (No border), Bottom: (No
border), Left: (No border), Right: (No border), Between : (No
border), Tab stops: 7.96 cm, Centred + 15.92 cm, Right

1174 Maksyutov, S., Oda, T., Saito, M., Janardanan, R., Belikov, D., Kaiser, J. W., Zhuravlev, R., Ganshin, A., Valsala, V. K.,
1175 Andrews, A., Chmura, L., Dlugokencky, E., Haszpra, L., Langenfelds, R. L., Machida, T., Nakazawa, T., Ramonet, M.,
1176 Sweeney, C., and Worthy, D.: Technical note: A high-resolution inverse modelling technique for estimating surface CO₂
1177 fluxes based on the NIES-TM-FLEXPART coupled transport model and its adjoint, *Atmospheric Chem. Phys.*, 21, 1245–
1178 1266, <https://doi.org/10.5194/acp-21-1245-2021>, 2021.

1179 McNicol, G., Fluet-Chouinard, E., Ouyang, Z., Knox, S., Zhang, Z., Aalto, T., Bansal, S., Chang, K.-Y., Chen, M.,
1180 Delwiche, K., Feron, S., Goeckede, M., Liu, J., Malhotra, A., Melton, J. R., Riley, W., Vargas, R., Yuan, K., Ying, Q., Zhu,
1181 Q., Alekseychik, P., Aurela, M., Billesbach, D. P., Campbell, D. I., Chen, J., Chu, H., Desai, A. R., Euskirchen, E.,
1182 Goodrich, J., Griffis, T., Helbig, M., Hirano, T., Iwata, H., Jurasinski, G., King, J., Koebsch, F., Kolka, R., Krauss, K.,
1183 Lohila, A., Mammarella, I., Nilson, M., Noormets, A., Oechel, W., Peichl, M., Sachs, T., Sakabe, A., Schulze, C.,
1184 Sonntag, O., Sullivan, R. C., Tuittila, E.-S., Ueyama, M., Vesala, T., Ward, E., Wille, C., Wong, G. X., Zona, D.,
1185 Windham-Myers, L., Poulter, B., and Jackson, R. B.: Upscaling Wetland Methane Emissions From the FLUXNET-CH₄
1186 Eddy Covariance Network (UpCH₄ v1.0): Model Development, Network Assessment, and Budget Comparison, *AGU Adv.*,
1187 4, e2023AV000956, <https://doi.org/10.1029/2023AV000956>, 2023.

1188 Melton, J. R. and Arora, V. K.: Competition between plant functional types in the Canadian Terrestrial Ecosystem Model
1189 (CTEM) v. 2.0, *Geosci. Model Dev.*, 9, 323–361, <https://doi.org/10.5194/gmd-9-323-2016>, 2016.

1190 Nisbet, E. G., Manning, M. R., Dlugokencky, E. J., Michel, S. E., Lan, X., Röckmann, T., Denier van der Gon, H. A. C.,
1191 Schmitt, J., Palmer, P. I., Dyonisius, M. N., Oh, Y., Fisher, R. E., Lowry, D., France, J. L., White, J. W. C., Brailsford, G.,
1192 and Bromley, T.: Atmospheric Methane: Comparison Between Methane's Record in 2006–2022 and During Glacial
1193 Terminations, *Glob. Biogeochem. Cycles*, 37, e2023GB007875, <https://doi.org/10.1029/2023GB007875>, 2023.

1194 Niwa, Y., Ishijima, K., Ito, A., and Iida, Y.: Toward a long-term atmospheric CO₂ inversion for elucidating natural carbon
1195 fluxes: technical notes of NISMOM-CO₂ v2021.1, *Prog. Earth Planet. Sci.*, 9, 42, [https://doi.org/10.1186/s40645-022-00502-](https://doi.org/10.1186/s40645-022-00502-6)
1196 6, 2022.

1197 Niwa, Y., Tohjima, Y., Terao, Y., Saeki, T., Ito, A., Umezawa, T., Yamada, K., Sasakawa, M., Machida, T., Nakaoka, S.-I.,
1198 Nara, H., Tanimoto, H., Mukai, H., Yoshida, Y., Morimoto, S., Takatsuji, S., Tsuboi, K., Sawa, Y., Matsueda, H., Ishijima,
1199 K., Fujita, R., Goto, D., Lan, X., Schuldt, K., Heliasz, M., Biermann, T., Chmura, L., Necki, J., Xueref-Remy, I., and
1200 Sferlazzo, D.: Multi-observational estimation of regional and sectoral emission contributions to the persistent high growth
1201 rate of atmospheric CH₄ for 2020–2022, *Atmospheric Chem. Phys.*, 25, 6757–6785, [https://doi.org/10.5194/acp-25-6757-](https://doi.org/10.5194/acp-25-6757-2025)
1202 2025, 2025.

1203 Parker, R. J., Boesch, H., McNorton, J., Comyn-Platt, E., Gloor, M., Wilson, C., Chipperfield, M. P., Hayman, G. D., and
1204 Bloom, A. A.: Evaluating year-to-year anomalies in tropical wetland methane emissions using satellite CH₄ observations,
1205 *Remote Sens. Environ.*, 211, 261–275, <https://doi.org/10.1016/j.rse.2018.02.011>, 2018.

1206 Patra, P. K., Takigawa, M., Watanabe, S., Chandra, N., Ishijima, K., and Yamashita, Y.: Improved Chemical Tracer
1207 Simulation by MIROC4.0-based Atmospheric Chemistry-Transport Model (MIROC4-ACTM), *SOLA*, 14, 91–96,
1208 <https://doi.org/10.2151/sola.2018-016>, 2018.

1209 Peng, S., Lin, X., Thompson, R. L., Xi, Y., Liu, G., Hauglustaine, D., Lan, X., Poulter, B., Ramonet, M., Saunio, M., Yin,
1210 Y., Zhang, Z., Zheng, B., and Ciais, P.: Wetland emission and atmospheric sink changes explain methane growth in 2020,
1211 *Nature*, 612, 477–482, <https://doi.org/10.1038/s41586-022-05447-w>, 2022.

Formatted: Font colour: Black
Formatted: Normal, Space Before: 14 pt, After: 14 pt,
Border: Top: (No border), Bottom: (No border), Left: (No
border), Right: (No border), Between : (No border)

Formatted: Font colour: Black
Formatted: Normal, Space Before: 14 pt, After: 14 pt,
Border: Top: (No border), Bottom: (No border), Left: (No
border), Right: (No border), Between : (No border)

Deleted: 26
Formatted: Font colour: Black
Formatted: Normal, Border: Top: (No border), Bottom: (No
border), Left: (No border), Right: (No border), Between : (No
border), Tab stops: 7.96 cm, Centred + 15.92 cm, Right

1212 Pu, T., Gerlein-Safdi, C., Xiong, Y., Li, M., Kort, E. A., and Bloom, A. A.: Berkeley-RWAWC: A New CYGNSS-Based
1213 Watermask Unveils Unique Observations of Seasonal Dynamics in the Tropics, *Water Resour. Res.*, 60, e2024WR037060,
1214 <https://doi.org/10.1029/2024WR037060>, 2024.

1215 [Qu, Z., Jacob, D. J., Bloom, A. A., Worden, J. R., Parker, R. J., and Boesch, H.: Inverse modeling of 2010–2022 satellite
1216 observations shows that inundation of the wet tropics drove the 2020–2022 methane surge, *Proc. Natl. Acad. Sci.*, 121,
1217 e2402730121, <https://doi.org/10.1073/pnas.2402730121>, 2024.](#)

1218 [Quinn, C. A., Colligan, T., Ward, E. J., East, J. D., Lim, Y., Lee, E., Koster, R. D., and Poulter, B.: Amazonia Wetland
1219 Methane Emission Decrease in 2023: Seasonal Forecasting of Global Wetlands Highlights Monitoring Targets in Critical
1220 Ecosystems, *J. Adv. Model. Earth Syst.*, 17, e2025MS005510, <https://doi.org/10.1029/2025MS005510>, 2025.](#)

1221 Riley, W. J., Subin, Z. M., Lawrence, D. M., Swenson, S. C., Torn, M. S., Meng, L., Mahowald, N. M., and Hess, P.:
1222 Barriers to predicting changes in global terrestrial methane fluxes: analyses using CLM4Me, a methane biogeochemistry
1223 model integrated in CESM, *Biogeosciences*, 8, 1925–1953, <https://doi.org/10.5194/bg-8-1925-2011>, 2011.

1224 Ringeval, B., Friedlingstein, P., Koven, C., Ciais, P., de Noblet-Ducoudré, N., Decharme, B., and Cadule, P.: Climate-CH4
1225 feedback from wetlands and its interaction with the climate-CO2 feedback, *Biogeosciences*, 8, 2137–2157,
1226 <https://doi.org/10.5194/bg-8-2137-2011>, 2011.

1227 Roberts, C. D., Senan, R., Molteni, F., Boussetta, S., Mayer, M., and Keeley, S. P. E.: Climate model configurations of the
1228 ECMWF Integrated Forecasting System (ECMWF-IFS cycle 43r1) for HighResMIP, *Geosci. Model Dev.*, 11, 3681–3712,
1229 <https://doi.org/10.5194/gmd-11-3681-2018>, 2018.

1230 Saunio, M., Stavert, A. R., Poulter, B., Bousquet, P., Canadell, J. G., Jackson, R. B., Raymond, P. A., Dlugokencky, E. J.,
1231 Houweling, S., Patra, P. K., Ciais, P., Arora, V. K., Bastviken, D., Bergamaschi, P., Blake, D. R., Brailsford, G., Bruhwiler,
1232 L., Carlson, K. M., Carrol, M., Castaldi, S., Chandra, N., Crevoisier, C., Crill, P. M., Covey, K., Curry, C. L., Etiope, G.,
1233 Frankenberg, C., Gedney, N., Hegglin, M. I., Höglund-Isaksson, L., Hugelius, G., Ishizawa, M., Ito, A., Janssens-Maenhout,
1234 G., Jensen, K. M., Joos, F., Kleinen, T., Krummel, P. B., Langenfelds, R. L., Laruelle, G. G., Liu, L., Machida, T.,
1235 Maksyutov, S., McDonald, K. C., McNorton, J., Miller, P. A., Melton, J. R., Morino, I., Müller, J., Murguia-Flores, F., Naik,
1236 V., Niwa, Y., Noce, S., O'Doherty, S., Parker, R. J., Peng, C., Peng, S., Peters, G. P., Prigent, C., Prinn, R., Ramonet, M.,
1237 Regnier, P., Riley, W. J., Rosentreter, J. A., Segers, A., Simpson, I. J., Shi, H., Smith, S. J., Steele, L. P., Thornton, B. F.,
1238 Tian, H., Tohjima, Y., Tubiello, F. N., Tsuruta, A., Viovy, N., Voulgarakis, A., Weber, T. S., van Weele, M., van der Werf,
1239 G. R., Weiss, R. F., Worthy, D., Wunch, D., Yin, Y., Yoshida, Y., Zhang, W., Zhang, Z., Zhao, Y., Zheng, B., Zhu, Q., Zhu,
1240 Q., and Zhuang, Q.: The Global Methane Budget 2000–2017, *Earth Syst. Sci. Data*, 12, 1561–1623,
1241 <https://doi.org/10.5194/essd-12-1561-2020>, 2020.

1242 Saunio, M., Martinez, A., Poulter, B., Zhang, Z., Raymond, P. A., Regnier, P., Canadell, J. G., Jackson, R. B., Patra, P. K.,
1243 Bousquet, P., Ciais, P., Dlugokencky, E. J., Lan, X., Allen, G. H., Bastviken, D., Beerling, D. J., Belikov, D. A., Blake, D.
1244 R., Castaldi, S., Crippa, M., Deemer, B. R., Dennison, F., Etiope, G., Gedney, N., Höglund-Isaksson, L., Holgerson, M. A.,
1245 Hopcroft, P. O., Hugelius, G., Ito, A., Jain, A. K., Janardanan, R., Johnson, M. S., Kleinen, T., Krummel, P. B., Lauerwald,
1246 R., Li, T., Liu, X., McDonald, K. C., Melton, J. R., Mühle, J., Müller, J., Murguia-Flores, F., Niwa, Y., Noce, S., Pan, S.,
1247 Parker, R. J., Peng, C., Ramonet, M., Riley, W. J., Rocher-Ros, G., Rosentreter, J. A., Sasakawa, M., Segers, A., Smith, S. J.,
1248 Stanley, E. H., Thanwerdas, J., Tian, H., Tsuruta, A., Tubiello, F. N., Weber, T. S., van der Werf, G. R., Worthy, D. E. J., Xi,
1249 Y., Yoshida, Y., Zhang, W., Zheng, B., Zhu, Q., Zhu, Q., and Zhuang, Q.: Global Methane Budget 2000–2020, *Earth Syst.*
1250 *Sci. Data*, 17, 1873–1958, <https://doi.org/10.5194/essd-17-1873-2025>, 2025.

Formatted: Font colour: Black

Formatted: Normal, Space Before: 14 pt, After: 14 pt,
Border: Top: (No border), Bottom: (No border), Left: (No
border), Right: (No border), Between : (No border)

Deleted: 27

Formatted: Font colour: Black

Formatted: Normal, Border: Top: (No border), Bottom: (No
border), Left: (No border), Right: (No border), Between : (No
border), Tab stops: 7.96 cm, Centred + 15.92 cm, Right

- 1251 Shu, S., Jain, A. K., and Kheshgi, H. S.: Investigating Wetland and Nonwetland Soil Methane Emissions and Sinks Across
1252 the Contiguous United States Using a Land Surface Model, *Glob. Biogeochem. Cycles*, 34, e2019GB006251,
1253 <https://doi.org/10.1029/2019GB006251>, 2020.
- 1254 Spahni, R., Wania, R., Neef, L., van Weele, M., Pison, I., Bousquet, P., Frankenberg, C., Foster, P. N., Joos, F., Prentice, I.
1255 C., and van Velthoven, P.: Constraining global methane emissions and uptake by ecosystems, *Biogeosciences*, 8, 1643–
1256 1665, <https://doi.org/10.5194/bg-8-1643-2011>, 2011.
- 1257 Stavert, A. R., Saunio, M., Canadell, J. G., Poulter, B., Jackson, R. B., Regnier, P., Lauerwald, R., Raymond, P. A., Allen,
1258 G. H., Patra, P. K., Bergamaschi, P., Bousquet, P., Chandra, N., Ciais, P., Gustafson, A., Ishizawa, M., Ito, A., Kleinen, T.,
1259 Maksyutov, S., McNorton, J., Melton, J. R., Müller, J., Niwa, Y., Peng, S., Riley, W. J., Segers, A., Tian, H., Tsuruta, A.,
1260 Yin, Y., Zhang, Z., Zheng, B., and Zhuang, Q.: Regional trends and drivers of the global methane budget, *Glob. Change
1261 Biol.*, 28, 182–200, <https://doi.org/10.1111/gcb.15901>, 2022.
- 1262 Stocker, B. D., Spahni, R., and Joos, F.: DYPTOP: a cost-efficient TOPMODEL implementation to simulate sub-grid spatio-
1263 temporal dynamics of global wetlands and peatlands, *Geosci. Model Dev.*, 7, 3089–3110, <https://doi.org/10.5194/gmd-7-3089-2014>, 2014.
- 1265 Thanwerdas, J., Saunio, M., Berchet, A., Pison, I., Vaughn, B. H., Michel, S. E., and Bousquet, P.: Variational inverse
1266 modeling within the Community Inversion Framework v1.1 to assimilate $\delta^{13}\text{C}(\text{CH}_4)$ and CH_4 : a case study with model
1267 LMDz-SACS, *Geosci. Model Dev.*, 15, 4831–4851, <https://doi.org/10.5194/gmd-15-4831-2022>, 2022.
- 1268 Tian, T., Yang, S., Hoyer, J. L., Nielsen-Englyst, P., and Singha, S.: Cooler Arctic surface temperatures simulated by climate
1269 models are closer to satellite-based data than the ERA5 reanalysis, *Commun. Earth Environ.*, 5, 111,
1270 <https://doi.org/10.1038/s43247-024-01276-z>, 2024.
- 1271 Toet, S., Ineson, P., Peacock, S., and Ashmore, M.: Elevated ozone reduces methane emissions from peatland mesocosms,
1272 *Glob. Change Biol.*, 17, 288–296, <https://doi.org/10.1111/j.1365-2486.2010.02267.x>, 2011.
- 1273 Tsuruta, A., Aalto, T., Backman, L., Hakkarainen, J., van der Laan-Luijckx, I. T., Krol, M. C., Spahni, R., Houweling, S.,
1274 Laine, M., Dlugokencky, E., Gomez-Pelaez, A. J., van der Schoot, M., Langenfelds, R., Ellul, R., Arduini, J., Apadula, F.,
1275 Gerbig, C., Feist, D. G., Kivi, R., Yoshida, Y., and Peters, W.: Global methane emission estimates for 2000–2012 from
1276 CarbonTracker Europe-CH4 v1.0, *Geosci. Model Dev.*, 10, 1261–1289, <https://doi.org/10.5194/gmd-10-1261-2017>, 2017.
- 1277 Tyystjärvi, V., Markkanen, T., Backman, L., Raivonen, M., Leppänen, A., Li, X., Ojanen, P., Minkkinen, K., Hautala, R.,
1278 Peltoniemi, M., Anttila, J., Laiho, R., Lohila, A., Mäkipää, R., and Aalto, T.: Future methane fluxes of peatlands are
1279 controlled by management practices and fluctuations in hydrological conditions due to climatic variability, *Biogeosciences*,
1280 21, 5745–5771, <https://doi.org/10.5194/bg-21-5745-2024>, 2024.
- 1281 Wang, F., Maksyutov, S., Tsuruta, A., Janardanan, R., Ito, A., Sasakawa, M., Machida, T., Morino, I., Yoshida, Y., Kaiser, J.
1282 W., Janssens-Maenhout, G., Dlugokencky, E. J., Mammarella, I., Lavric, J. V., and Matsunaga, T.: Methane Emission
1283 Estimates by the Global High-Resolution Inverse Model Using National Inventories, *Remote Sens.*, 11, 2489,
1284 <https://doi.org/10.3390/rs11212489>, 2019.
- 1285 Xu, X., Sharma, P., Shu, S., Lin, T.-S., Ciais, P., Tubiello, F. N., Smith, P., Campbell, N., and Jain, A. K.: Global
1286 greenhouse gas emissions from animal-based foods are twice those of plant-based foods, *Nat. Food*, 2, 724–732,
1287 <https://doi.org/10.1038/s43016-021-00358-x>, 2021.

Deleted: 28**Formatted:** Font colour: Black**Formatted:** Normal, Border: Top: (No border), Bottom: (No border), Left: (No border), Right: (No border), Between : (No border), Tab stops: 7.96 cm, Centred + 15.92 cm, Right

- 1288 Yuan, K., Zhu, Q., Li, F., Riley, W. J., Torn, M., Chu, H., McNicol, G., Chen, M., Knox, S., Delwiche, K., Wu, H.,
1289 Baldocchi, D., Ma, H., Desai, A. R., Chen, J., Sachs, T., Ueyama, M., Sonnentag, O., Helbig, M., Tuittila, E.-S., Jurasinski,
1290 G., Koepsch, F., Campbell, D., Schmid, H. P., Lohila, A., Goeckede, M., Nilsson, M. B., Friborg, T., Jansen, J., Zona, D.,
1291 Euskirchen, E., Ward, E. J., Bohrer, G., Jin, Z., Liu, L., Iwata, H., Goodrich, J., and Jackson, R.: Causality guided machine
1292 learning model on wetland CH₄ emissions across global wetlands, *Agric. For. Meteorol.*, 324, 109115,
1293 <https://doi.org/10.1016/j.agrformet.2022.109115>, 2022.
- 1294 Yuan, K., Li, F., McNicol, G., Chen, M., Hoyt, A., Knox, S., Riley, W. J., Jackson, R., and Zhu, Q.: Boreal–Arctic wetland
1295 methane emissions modulated by warming and vegetation activity, *Nat. Clim. Change*, 14, 282–288,
1296 <https://doi.org/10.1038/s41558-024-01933-3>, 2024.
- 1297 Yvon-Durocher, G., Allen, A. P., Bastviken, D., Conrad, R., Gudas, C., St-Pierre, A., Thanh-Duc, N., and del Giorgio, P.
1298 A.: Methane fluxes show consistent temperature dependence across microbial to ecosystem scales, *Nature*, 507, 488–491,
1299 <https://doi.org/10.1038/nature13164>, 2014.
- 1300 Zhang, Z., Zimmermann, N. E., Kaplan, J. O., and Poulter, B.: Modeling spatiotemporal dynamics of global wetlands:
1301 comprehensive evaluation of a new sub-grid TOPMODEL parameterization and uncertainties, *Biogeosciences*, 13, 1387–
1302 1408, <https://doi.org/10.5194/bg-13-1387-2016>, 2016.
- 1303 Zhang, Z., Poulter, B., Feldman, A. F., Ying, Q., Ciais, P., Peng, S., and Li, X.: Recent intensification of wetland methane
1304 feedback, *Nat. Clim. Change*, 13, 430–433, <https://doi.org/10.1038/s41558-023-01629-0>, 2023.
- 1305 Zhang, Z., Poulter, B., Melton, J. R., Riley, W. J., Allen, G. H., Beerling, D. J., Bousquet, P., Canadell, J. G., Fluet-
1306 Chouinard, E., Ciais, P., Gedney, N., Hopcroft, P. O., Ito, A., Jackson, R. B., Jain, A. K., Jensen, K., Joos, F., Kleinen, T.,
1307 Knox, S. H., Li, T., Li, X., Liu, X., McDonald, K., McNicol, G., Miller, P. A., Müller, J., Patra, P. K., Peng, C., Peng, S.,
1308 Qin, Z., Riggs, R. M., Saunio, M., Sun, Q., Tian, H., Xu, X., Yao, Y., Xi, Y., Zhang, W., Zhu, Q., Zhu, Q., and Zhuang, Q.:
1309 Ensemble estimates of global wetland methane emissions over 2000–2020, *Biogeosciences*, 22, 305–321,
1310 <https://doi.org/10.5194/bg-22-305-2025>, 2025.
- 1311 Zheng, B., Chevallier, F., Ciais, P., Yin, Y., and Wang, Y.: On the Role of the Flaming to Smoldering Transition in the
1312 Seasonal Cycle of African Fire Emissions, *Geophys. Res. Lett.*, 45, 11,998–12,007, <https://doi.org/10.1029/2018GL079092>,
1313 2018a.
- 1314 Zheng, B., Chevallier, F., Ciais, P., Yin, Y., Deeter, M. N., Worden, H. M., Wang, Y., Zhang, Q., and He, K.: Rapid decline
1315 in carbon monoxide emissions and export from East Asia between years 2005 and 2016, *Environ. Res. Lett.*, 13, 044007,
1316 <https://doi.org/10.1088/1748-9326/aab2b3>, 2018b.
- 1317 Zheng, B., Chevallier, F., Yin, Y., Ciais, P., Fortems-Cheiney, A., Deeter, M. N., Parker, R. J., Wang, Y., Worden, H. M.,
1318 and Zhao, Y.: Global atmospheric carbon monoxide budget 2000–2017 inferred from multi-species atmospheric inversions,
1319 *Earth Syst. Sci. Data*, 11, 1411–1436, <https://doi.org/10.5194/essd-11-1411-2019>, 2019.
- 1320 Zhu, Q., Yuan, K., Li, F., Riley, W. J., Hoyt, A., Jackson, R., McNicol, G., Chen, M., Knox, S. H., Briner, O., Beerling, D.,
1321 Gedney, N., Hopcroft, P. O., Ito, A., Jain, A. K., Jensen, K., Kleinen, T., Li, T., Liu, X., McDonald, K. C., Melton, J. R.,
1322 Miller, P. A., Müller, J., Peng, C., Poulter, B., Qin, Z., Peng, S., Tian, H., Xu, X., Yao, Y., Xi, Y., Zhang, Z., Zhang, W.,
1323 Zhu, Q., and Zhuang, Q.: Critical needs to close monitoring gaps in pan-tropical wetland CH₄ emissions, *Environ. Res. Lett.*,
1324 19, 114046, <https://doi.org/10.1088/1748-9326/ad8019>, 2024.

Deleted: 29ⁿ**Formatted:** Font colour: Black**Formatted:** Normal, Border: Top: (No border), Bottom: (No border), Left: (No border), Right: (No border), Between : (No border), Tab stops: 7.96 cm, Centred + 15.92 cm, Right

1325
1326
1327
1328

1329
1330
1331
1332

Zhu, Q., Jacob, D. J., Yuan, K., Li, F., Runkle, B. R. K., Chen, M., Bloom, A. A., Poulter, B., East, J. D., Riley, W. J., McNicol, G., Worden, J., Frankenberg, C., and Halabisky, M.: Advancements and opportunities to improve bottom-up estimates of global wetland methane emissions, Environ. Res. Lett., 20, 023001, <https://doi.org/10.1088/1748-9326/adad02>, 2025.

Zona, D., Gioli, B., Commane, R., Lindaas, J., Wofsy, S. C., Miller, C. E., Dinardo, S. J., Dengel, S., Sweeney, C., Karion, A., Chang, R. Y.-W., Henderson, J. M., Murphy, P. C., Goodrich, J. P., Moreaux, V., Liljedahl, A., Watts, J. D., Kimball, J. S., Lipson, D. A., and Oechel, W. C.: Cold season emissions dominate the Arctic tundra methane budget, Proc. Natl. Acad. Sci., 113, 40–45, <https://doi.org/10.1073/pnas.1516017113>, 2016.

Formatted: Font colour: Black
Formatted: Normal, Border: Top: (No border), Bottom: (No border), Left: (No border), Right: (No border), Between : (No border)

Deleted: 30
Formatted: Font colour: Black
Formatted: Normal, Border: Top: (No border), Bottom: (No border), Left: (No border), Right: (No border), Between : (No border), Tab stops: 7.96 cm, Centred + 15.92 cm, Right

Page 1: [1] Formatted	Mengze Li	22/04/2026 00:22:00
------------------------------	------------------	----------------------------

Font colour: Black

Page 1: [2] Formatted	Mengze Li	22/04/2026 00:22:00
------------------------------	------------------	----------------------------

Normal, Border: Top: (No border), Bottom: (No border), Left: (No border), Right: (No border), Between : (No border), Tab stops: 7.96 cm, Centred + 15.92 cm, Right

Page 13: [3] Deleted	Mengze Li	22/04/2026 00:22:00
-----------------------------	------------------	----------------------------

Page 13: [4] Formatted	Mengze Li	22/04/2026 00:22:00
-------------------------------	------------------	----------------------------

Font: 11 pt

Page 13: [5] Formatted	Mengze Li	22/04/2026 00:22:00
-------------------------------	------------------	----------------------------

Formatted

Page 13: [5] Formatted	Mengze Li	22/04/2026 00:22:00
-------------------------------	------------------	----------------------------

Formatted

Page 13: [6] Formatted	Mengze Li	22/04/2026 00:22:00
-------------------------------	------------------	----------------------------

Formatted

Page 13: [7] Formatted	Mengze Li	22/04/2026 00:22:00
-------------------------------	------------------	----------------------------

Formatted

Page 13: [7] Formatted	Mengze Li	22/04/2026 00:22:00
-------------------------------	------------------	----------------------------

Formatted

Page 13: [7] Formatted	Mengze Li	22/04/2026 00:22:00
-------------------------------	------------------	----------------------------

Formatted

Page 13: [8] Formatted	Mengze Li	22/04/2026 00:22:00
-------------------------------	------------------	----------------------------

Formatted

Page 13: [9] Formatted	Mengze Li	22/04/2026 00:22:00
-------------------------------	------------------	----------------------------

Formatted

Page 13: [9] Formatted	Mengze Li	22/04/2026 00:22:00
-------------------------------	------------------	----------------------------

Formatted

Page 13: [10] Formatted	Mengze Li	22/04/2026 00:22:00
--------------------------------	------------------	----------------------------

Formatted

Page 13: [11] Formatted	Mengze Li	22/04/2026 00:22:00
--------------------------------	------------------	----------------------------

Formatted

Page 13: [12] Formatted	Mengze Li	22/04/2026 00:22:00
--------------------------------	------------------	----------------------------

Formatted

Page 13: [13] Formatted	Mengze Li	22/04/2026 00:22:00
--------------------------------	------------------	----------------------------

Formatted

Page 13: [14] Formatted	Mengze Li	22/04/2026 00:22:00
--------------------------------	------------------	----------------------------

Formatted

Page 13: [15] Formatted	Mengze Li	22/04/2026 00:22:00
--------------------------------	------------------	----------------------------

Formatted

Page 13: [16] Formatted	Mengze Li	22/04/2026 00:22:00
--------------------------------	------------------	----------------------------

Formatted

Page 13: [17] Formatted	Mengze Li	22/04/2026 00:22:00
Formatted		
Page 13: [18] Formatted	Mengze Li	22/04/2026 00:22:00
Formatted		
Page 13: [19] Formatted	Mengze Li	22/04/2026 00:22:00
Formatted		
Page 13: [20] Formatted	Mengze Li	22/04/2026 00:22:00
Formatted		
Page 13: [20] Formatted	Mengze Li	22/04/2026 00:22:00
Formatted		
Page 13: [21] Formatted	Mengze Li	22/04/2026 00:22:00
Formatted		
Page 13: [22] Formatted	Mengze Li	22/04/2026 00:22:00
Formatted		
Page 1: [23] Formatted	Mengze Li	22/04/2026 00:22:00
Normal, Border: Top: (No border), Bottom: (No border), Left: (No border), Right: (No border), Between : (No border), Tab stops: 7.96 cm, Centred + 15.92 cm, Right		
Page 14: [24] Formatted	Mengze Li	22/04/2026 00:22:00
Formatted		
Page 14: [24] Formatted	Mengze Li	22/04/2026 00:22:00
Formatted		
Page 14: [25] Formatted	Mengze Li	22/04/2026 00:22:00
Formatted		
Page 14: [25] Formatted	Mengze Li	22/04/2026 00:22:00
Formatted		
Page 14: [25] Formatted	Mengze Li	22/04/2026 00:22:00
Formatted		
Page 14: [26] Formatted	Mengze Li	22/04/2026 00:22:00
Formatted		
Page 14: [26] Formatted	Mengze Li	22/04/2026 00:22:00
Formatted		
Page 14: [27] Deleted	Mengze Li	22/04/2026 00:22:00
v		
Page 14: [28] Formatted	Mengze Li	22/04/2026 00:22:00
Formatted		
Page 14: [28] Formatted	Mengze Li	22/04/2026 00:22:00
Formatted		
Page 14: [28] Formatted	Mengze Li	22/04/2026 00:22:00
Formatted		
Page 14: [29] Deleted	Mengze Li	22/04/2026 00:22:00
v		
Page 14: [29] Deleted	Mengze Li	22/04/2026 00:22:00
v		
Page 14: [30] Deleted	Mengze Li	22/04/2026 00:22:00

▼
Page 14: [31] Deleted **Mengze Li** **22/04/2026 00:22:00**

▼
Page 14: [31] Deleted **Mengze Li** **22/04/2026 00:22:00**

▼
Page 18: [32] Deleted **Mengze Li** **22/04/2026 00:22:00**

▼